AD-A064 362 AIR FORCE INST OF TECH WRIGHT-PATTERSON AFB OHIO SCH--ETC F/G 20/12
ELECTRICAL EFFECTS OF THREE DIFFERENT ENCAPSULANTS ON ION IMPLA--ETC(U)
DEC 78 S D BREAULT

UNCLASSIFIED AFIT/GE/EE/78-19 NL

1 OF 1
AD
A064362

END
DATE
FILMED
4 -79
DDC

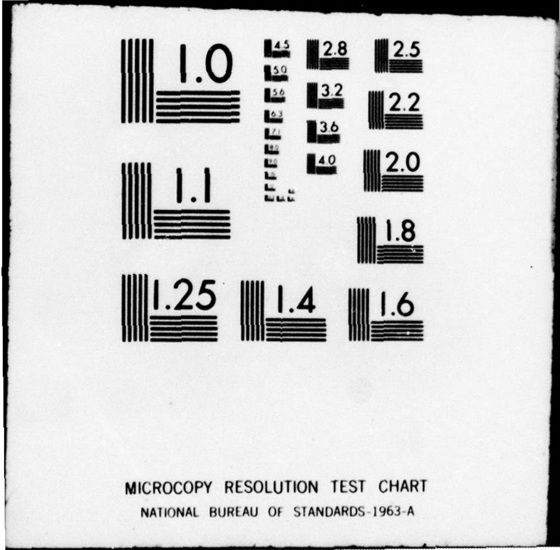
1.0
1.1
1.25
1.4
1.6
1.8
2.0
2.2
2.5
2.8
3.2
3.6
4.0
MICROCOPY RESOLUTION TEST CHART
NATIONAL BUREAU OF STANDARDS-1963-A

AFIT/GE/EE/78-19

LEVEL II

AD A064362

DDC FILE COPY

See back page for 1473

ELECTRICAL EFFECTS OF THREE DIFFERENT ENCAPSULANTS ON ION IMPLANTED GaAs

THESIS

AFIT/GE/EE/78-19 Simeon D. Breault
Captain USAF

DDC
FEB 9 1979
A

Approved for public release; distribution unlimited.

79 01 30 141

AFIT/GE/EE/78-19

ELECTRICAL EFFECTS OF THREE DIFFERENT ENCAPSULANTS ON ION IMPLANTED GaAs

THESIS

Presented to the Faculty of the School of Engineering
of the Air Force Institute of Technology

Air Training Command

in Partial Fulfillment of the
Requirements for the Degree of

Master of Science

by

Simeon D. Breault, B.S.
Captain USAF

Graduate Electrical Engineering

December 1978

Approved for public release; distribution unlimited.

Preface

This study was sponsored by the Electronics Research Branch of the Air Force Avionics Laboratory, Wright-Patterson Air Force Base, Ohio. It is part of their continuing investigation into the electrical and physical properties of ion implanted GaAs. The work, a study of the effectiveness of different encapsulants, was done in support of work being done at this laboratory, as well as other Air Force laboratories.

I am very grateful to several people, for without their help and guidance this investigation could not have been accomplished. I especially want to thank Dr. Y. S. Park, my sponsor, and Y. K. Yeo who guided my experiments. I also want to thank Jim Ehret, who implanted my samples, Charlie Geesner and Rick Patton, who capped my samples, and my wife Monique, who typed my thesis. Finally, I want to thank my thesis advisor, Capt. Mike Borky.

ACCESSION for
NTIS White Section
DDC Buff Section
UNANNOUNCED
JUSTIFICATION
BY
DISTRIBUTION/AVAILABILITY CODES
Dist. AVAIL. and/or SPECIAL
A

Contents

Preface ii

List of Figures iv

List of Tables v

Abstract vi

I. Introduction 1

Thesis Objective and Scope 2
Results Summary 3
Sequence of Presentation 4

II. Background 5

Ion Implantation 5
Lindhard, Sharff and Shiott Theory 6
Previous Studies of Encapsulation Effectiveness 8

III. Experimental Procedure 11

Sample Preparation 11
Data Acquisition 14

IV. Experimental Results 20

Mg-Implants 20
S-Implants 29

V. Discussion of Experimental Results 36

VI. Summary and Recommendations 40

Bibliography 42

Appendix A: Other Electrical Profiles 44

Vita 53

List of Figures

Figures		Page
1	Van der Pauw Measurement System	15
2	Sample Connections	16
3	Surface Concentration and Mobility as Functions of Dose	24
4	Carrier Concentration and Mobility Profile	26
5	Electrical Profile Comparison for Different Encapsulants	27
6	Electrical Profile Comparison for Different Encapsulants	28
7	Surface Concentration and Mobility as Functions of Dose	33
8	Electrical Profile Comparison for Different Encapsulants	35
9	Carrier Concentration and Mobility Profile	45
10	Carrier Concentration and Mobility Profile	46
11	Carrier Concentration and Mobility Profile	47
12	Carrier Concentration and Mobility Profile	48
13	Carrier Concentration and Mobility Profile	49
14	Carrier Concentration and Mobility Profile	50
15	Carrier Concentration and Mobility Profile	51
16	Carrier Concentration and Mobility Profile	52

List of Tables

Table		Page
I	Previous Studies of Encapsulation Effects . . .	8
II	Pyrolitic Si_3N_4 caps -- Magnesium Implants . .	20
III	Pyrolitic SiO_2 caps -- Magnesium Implants . . .	21
IV	Plasma Si_3N_4 caps -- Magnesium Implants	21
V	Electrical Activation Efficiencies (%) for Different Encapsulants -- Magnesium Implants .	23
VI	Pyrolitic Si_3N_4 caps -- Sulfur Implants	30
VII	Pyrolitic SiO_2 caps -- Sulfur Implants	31
VIII	Plasma Si_3N_4 caps -- Sulfur Implants	31
IX	Electrical Activation Efficiencies (%) for Different Encapsulants -- Sulfur Implants . . .	32

Abstract

A comparative study was done of the effectiveness of three different encapsulants for annealing ion-implanted GaAs. The three encapsulants studied were pyrolitic Si_3N_4 and SiO_2, and plasma Si_3N_4. The study was limited to magnesium and sulfur implants done at room temperature with an implant energy of 120 keV. The implants were made into Cr-doped, semi-insulating GaAs substrates to doses ranging from $3x10^{12}$ to $1x10^{15}cm^{-2}$. Annealing was done in a flowing hydrogen atmosphere at 850°C for 15 minutes. Comparisons of effectiveness were made on the basis of electrical activation efficiency and electrical profile measurements which were taken using a guarded Van der Pauw measurement system.

There was not a great deal of difference in the observed electrical activation efficiencies produced by the three different encapsulants. Plasma Si_3N_4 caps generally produced the highest activations, but were prone to pitting during annealing. The three encapsulants produced nearly identical electrical profiles, both for Mg and S implants. Contrary to previous studies, pyrolitic SiO_2 caps produced higher activations than pyrolitic Si_3N_4 caps for some doses of the S implants.

ELECTRICAL EFFECTS OF THREE DIFFERENT ENCAPSULANTS ON ION IMPLANTED GaAs

I. Introduction

Because of the technological problems associated with doping GaAs (and other III-V compound semiconductors) by conventional thermal diffusion methods commonly used in Si technology, ion implantation has become a common method for doping GaAs substrates (in wafer form). Ion implantation has already been successfuly used in the fabrication of microwave GaAs FETs. In the future, ion implantation may be used to fabricate digital integrated circuits made up of transfered electron devices on GaAs substrates; these circuits would theoretically be capable of logic rates in the GHz range. An alternative fabrication method is the growing of doped epitaxial layers on semi-insulating substrates and then selectively etching the doped layer to form device patterns. However, the growth of high quality epitaxial layers is not a simple process.

Ion implantation requires high temperature annealing after the implantation to remove the crystal lattice damage suffered by the substrate during implantation. Because GaAs begins to dissociate at temperatures above 500°C, a dielectric film, or encapsulant, is required to protect the substrate's implanted surface during annealing. As pointed out

in Chapter II, researchers have tried several different encapsulants with varying results.

Thesis Objective and Scope

The objective of this thesis was to perform a comparative study of the three encapsulants used by the Electronic Research Branch of the Air Force Avionics Laboratory (AFAL/DHR). The three encapsulants studied were pyrolitic silicon dioxide (SiO_2), pyrolitic silicon nitride (Si_3N_4), and plasma deposited Si_3N_4.

The study was done by measuring and comparing the electrical activations achieved using the three different encapsulants on samples of GaAs implanted with magnesium (Mg) and sulfur (S) to several doses. The doses used for Mg were $3x10^{12}$, $1x10^{13}$, $5x10^{13}$, $3x10^{14}$, and $1x10^{15}$ ions/cm^2; the doses used for S were $3x10^{12}$, $1x10^{13}$, $3x10^{13}$, $1x10^{14}$, and $3x10^{14}$ ions/cm^2. Electrical activation was determined by using the Van der Pauw technique to measure the sheet resistivity and sheet Hall coefficient of each sample. From these, the surface concentration and mobility of active carriers and the activation efficiency were computed (Ref 17). Active carrier vs. depth profiles were measured for Mg-implanted samples with doses of $5x10^{13}$ and $3x10^{14}$ ions/cm^2 and for S-implanted samples with a dose of $3x10^{13}$ ions/cm^2. The profiles were measured by combining the Van der Pauw measurements with layer removal by chemical etching.

Results Summary

This investigation showed that there was not a great deal of difference in the observed electrical activation efficiencies produced when the three different encapsulants are used. For the Mg-implanted samples, plasma Si_3N_4 encapsulated samples exhibited the highest electrical activations for almost all doses. The same was true for S-implanted samples.

Previous investigations had shown that because Ga outdiffusion was greater for SiO_2 caps than for Si_3N_4 caps, the former would be superior for p-type dopants (which accupy Ga vacancies) and the latter for n-type dopants (for which Ga vacancies serve as compensation complexes). This hypothesis was not supported by the data collected for this thesis. The activation observed for Mg-implanted (p-type) samples with Si_3N_4 caps (both pyrolitic and plasma) was generally nearly equal to or greater than the activation observed with SiO_2 caps. The activation observed for S-implanted samples (n-type) with pyrolitic SiO_2 caps was generally nearly equal to or greater than the activation observed with pyrolitic Si_3N_4 caps. (However, activations were higher still with plasma Si_3N_4 caps.)

Both Mg-implanted and S-implanted samples exhibited very similar electrical profiles for the different encapsulants. However, the observed peak in the profiles for the S-implanted samples was closer to the surface than what LSS theory predicted, while the peak in the profiles for the Mg-implan-

ted samples was deeper than predicted by LSS (which can be accounted for by diffusion during annealing). (LSS theory is briefly described in Chapter II.)

<u>Sequence of Presentation</u>

Chapter II provides background information for this thesis. It includes a short discussion of the basic concepts involved in ion implantation, a brief description of LSS theory, and a summary of the results of previous investigations which compare the effectiveness of different encapsulants. A description of how the samples used were prepared and of the experimental methods and processing techniques used to acquire data is given in Chapter III, including the cleaning methods, capping methods, and measurement techniques used during this study, and the equipment used. Chapter IV presents the data and results in tabular and graphical form. The results are then discussed and compared with previous results in Chapter V. Chapter VI concludes this thesis with a summary of the most significant results and recommendations for future studies.

II. Background

Ion Implantation

Ion implantation consists of bombarding a semiconductor substrate with high energy ions. The purpose of this process is to dope the semiconductor substrate to obtain a desired level and type of conductivity in a layer near the substrate's surface. To perform ion implantation the desired dopant species is ionized in a special chamber. The ions are then electrostatically accelerated and focused into a beam of specified energy, which eventually impacts on the substrate. However, before the beam impacts on the substrate, it is passed through a mass spectrometer which is tuned to the mass of the desired ion species. Thus a high degree of control over exactly what is being implanted into the substrate is possible. To insure that the desired ions are not deflected by stray molecules, the entire ion beam path is kept under a very high vacuum during the implantation process. Also, provisions are usually made to heat the target substrate since it has been shown that hot implantations can lead to higher doping efficiencies (Ref 5).

Ion implantation has several valuable characteristics for the doping of semiconductor substrates. Ion implantation can be done at relatively low temperatures. This feature is especially useful for the doping of compound semiconductors. (For example, GaAs begins to decompose at temperatures above 500 °C.) The amount of dopant implanted

into a substrate can easily be controlled by closely monitoring the ion beam current and time during the implantation. Special advantages of ion implantation with respect to masking include the use of evaporated or demountable metal masks, self-masking by gate structures (as in FETs), and the possibility of eliminating masks by establishing doping patterns on a substrate directly using computer controlled ion beams (Ref 1:3707).

Despite the advantages of ion implantation mentioned above, there are some complications unique to ion implantation. The physical processes taking place in ion implantation are very complex. A substantial amount of crystal lattice disorder, or damage, is produced by the incident ion beam in the substrate. To achieve electrical activation of the dopant, the crystal damage must be removed by annealing the sample at high temperatures (700 to 900 ^{o}C). Thus when implanting GaAs, it is necessary to cap the substrate prior to annealing to prevent the GaAs from decomposing at the high temperatures required.

<u>Lindhard, Sharff, and Shiott (LSS) Theory</u>

The incident ions lose their energy in the substrate as predicted by LSS theory for the stoping of heavy ions in an amorphous substrate. The density distribution or profile of the implanted ions predicted by LSS theory depends on the energy of the incident ions, their mass, the total dose, and the mass of the substrate ions.

The LSS theory predicts the concentration distribution

of implanted atoms in a amorphous solid. In application to semiconductor substrates, the amorphous solid is approximated by implanting along an axis which is not parallel to the axes of symmetry in the semiconductor crystal. For this thesis, implantations were made approximately 6° to 10° off the <100>direction. The LSS theory considers the stopping effect of the atoms in the substrate on the implanted ions through various kinetic energy loss mechanisms. As a result, the distribution of implanted ions is Gausian. The range, R_p (position of the peak in the distribution), and the standard deviation, ΔR_p, depend on the energy of the implanted ions, their mass, and the mass of the atoms in the substrate. Gibbons, et al. (Ref 21) have developed a computer program to calculate R_p and ΔR_p and have tabulated the results for various implants, energies, and substrates.

Once R_p and ΔR_p are known, the predicted concentration profile, N(x), of the implanted ions can be obtained from

$$N(x) = \frac{10^8 \phi}{R_p\sqrt{2\pi}} \exp\left[\frac{-(x-R_p)^2}{2\Delta R_p^2}\right] \qquad (1)$$

where x is the depth measured normal to the surface of the substrate in Å

ϕ = fluence, or ion dose, cm^{-2}

ΔR_p = standard deviation of the projected range, Å

R_p = projected range, Å.

Previous Studies of Encapsulation Effectiveness

Because GaAs dissociates at the temperatures required to anneal the damage induced during implantation, effective encapsulation is very important to achieving high levels of electrical activity. Because of its importance, much work has gone into studying encapsulation effects as shown by Table I. Table I illustrates that several materials have

Table I

Previous Studies of Encapsulation Effects

Ref no.	Encapsulant(s) studied
2	SiO_2, Si_3N_4 (sputtered)
3	SiO_2 (pyrolitic), Si_3N_4 (sputtered)
4	Al (evaporated)
5	Si_3N_4 (pyrolitic)
6	Ga_2O_3 (oxydation)
7	AlN (sputtered), Si_3N_4 (sputtered)
8	SiO_2 + Ga, SiO_2 (spun on, baked), Si_3N_4 (sputtered), AlN (sputtered)
9	SiO_2 (pyrolitic), Si_3N_4 (pyrolitic and sputtered)
10	Capless (controlled atmosphere)
11	Capless (controlled atmosphere)
12	Si_3N_4, AlON (sputtered)
13	Si_3N_4 (pyrolitic)
14	Si_3N_4, AlON (sputtered)
15	Si_3N_4 (plasma) under SiO_2 (CVD)

been studied as encapsulants for annealing ion-implanted GaAs. The most commonly used encapsulants are SiO_2 and Si_3N_4. The most commonly used methods of depositing these encapsulants are pyrolysis (or chemical vapor deposition -- CVD) and sputtering. All of the studies which compared SiO_2 and Si_3N_4 encapsulants on n-type-dopant implanted GaAs consistently show that samples capped with SiO_2 have lower doping efficiencies, which is believed to be a result of Ga outdiffusion through the cap. Si_3N_4 caps deposited by CVD or sputtering methods are reported to have adherence problems and are prone to pitting when annealed at very high temperatures (900°C). A newer technique of pyrolytically depositing Si_3N_4 allows reproducible annealing up to 950°C without any blistering or pealing of the cap. However, AlN coatings appear to have better adherence than Si_3N_4, while allowing comparable maximum electrical activation levels.

Less common methods of encapsulation have also been used with some success. Sealy, et al. (Ref 4), reported that the use of evaporated aluminum layers, 3000 angstroms thick, for encapsulation seems to provide more reproducible implantation results than Si_3N_4 or SiO_2 encapsulants. Also samples capped with Al had higher doping efficiencies. Sealy and D'Cruz (Ref 6) have reported producing uniform Ga_2O_3 layers by oxidation at 500 to 600°C. But when the native oxide was used as an encapsulant for implanted samples, reproducibility was poor and electrical activation generally lower than on samples capped with Al. Davies,

et al. (Ref 8) have reported improved electrical activation of group VI implants by incorporating Ga into SiO_2 encapsulants. This method proved detrimental to Si (group IV) implants, however.

Some researchers have even used "capless" annealing methods. Ref 10 describes a method of capless annealing involving placing the implanted face of a sample into a layer of crushed GaAs in the annealing furnace. Carrier profiles of the caplessly annealed samples were nearly identical to those of samples capped with Si_3N_4. Ref 11 describes the results of substituting a controlled atmosphere for the dielectric encapsulant normally used to protect the GaAs surface during high temperature annealing. The controlled atmosphere consists of H_2 gas plus As from a liquid GaAs source. Doping efficiencies of up to 86% were reported using this method.

In this thesis, pyrolytically deposited Si_3N_4 and SiO_2, and plasma deposited Si_3N_4 encapsulants were studied by measuring the electrical activations achieved using these three different encapsulants on implanted GaAs substrates. Chapter III next describes the experimental procedures used in this investigation.

III. Experimental Procedure

Sample Preparation

The GaAs samples used for this study were <100>-oriented, Cr-doped, semi-insulating, single-crystal substrates obtained from Crystal Specialties, Inc. The substrate wafers were scribed and broken into square samples about .5 cm on a side. Before implantation the samples were cleaned using the following procedure: 1) wash with 10% Aquasol soap solution, 2) rinse in flowing de-ionized water, 3) blow dry with inert gas (nitrogen or argon), 4) rinse in flowing trichloroethylene for 20 seconds, 5) rinse in flowing acetone for 20 seconds, 6) rinse in flowing methanol for 20 seconds, 7) blow dry with inert gas. To remove any oxide films and small scratches the samples were etched in a 3:1:1 solution by volume of H_2SO_4:30%H_2O_2:H_2O for 90 seconds.

All of the implantations were done with an ion energy of 120 keV at room temperature. The incident ion beam was directed at an angle of about 6° to 10° from the normal to the sample surfaces in order to minimize the ion channeling effect. The Mg-implanted samples had doses ranging from $3x10^{12}$ ions/cm^2 to $1x10^{15}$ ions/cm^2. The S-implanted samples had doses ranging from $3x10^{12}$ ions/cm^2 to $3x10^{14}$ ions/cm^2.

After implantation, the samples were again carefully cleaned using the same procedure described above, except no etching was done. Then the samples were capped, using

one of three encapsulants. Pyrolitic Si_3N_4 and SiO_2 were deposited using pyrolitic reactors based on an MIT Lincoln Laboratories design (Ref 16;26). The sample rested on a graphite strip in a small glass bell-jar chamber. The chamber was initially evacuated to remove impurities from the system, and then it was purged with nitrogen. As the chamber was being purged, the sample was brought to 200°C. After purging for a few minutes, controlled amounts of silane, SiH_4, and amonia, NH_3, which were diluted with equal amounts of nitrogen, were introduced to produce Si_3N_4 films (silane and oxygen were used to produce SiO_2 films). This mixture was added to the chamber through a nozzle directed down on the sample's surface. The sample was then quickly brought up to about 700°C (in 6 seconds) for 30 seconds, during which the gasses reacted to form a Si_3N_4 film about 1000Å thick (for 1000Å SiO_2 films, the sample temperature was 300°C for 5 minutes). Finally, the sample was quickly brought back to 200°C while the chamber was purged with nitrogen. The film thickness and refractive index was checked using a Gaetner Scientific, Inc. ellipsometer.

Plasma Si_3N_4 films were deposited using an RF plasma reactor. The sample to be capped was placed on a holder, which could be heated, in the reactor chamber. The chamber was then evacuated to a pressure of about $5x10^{-6}$ torr, while the sample was heated to 330°C. The plasma was ignited by an RF inductor (50 watts) to clean out the chamber

for a few minutes. A shutter over the sample prevented any film deposition at this time. The RF power was turned off and a small amount of silane gas was introduced. The chamber was again evacuated. Any oxygen left in the chamber, which could contaminate the capping film, was presumed to have combined with the silane and been swept out by the vacuum pump. When the pressure had dropped back down to about 5×10^{-6} torr, controlled amounts of silane and nitrogen were introduced into the reactor, the plasma was ignited, a timer was started, and the shutter was opened. The thickness of the film was controlled by the time allowed for the deposition. A film about 1000Å thick was produced in 10 minutes. When the alloted time had passed, the RF power was turned off and the chamber was evacuated again. After a few minutes, the chamber was vented with nitrogen and the sample removed.

After encapsulation, the samples were annealed in an H_2 ambient at 850°C for 15 minutes. The H_2 was burned on a platinum wire as it flowed out of the annealing furnace to prevent explosion.

The encapsulant was removed using a 48% reagent hydrofluoric acid, usually requiring about 3-5 minutes immersion for Si_3N_4 films and about 30 seconds for SiO_2 films. The samples were then rinsed in flowing de-ionized water and blown dry with N_2 gas.

Indium Contacts were next applied to the four corners of the samples using an ultrasonic soldering iron. The

contacts were sintered by heating the samples to 300°C for 5 minutes in an Ar ambient. Ohmicity of the contacts was checked using a curve tracer.

Data Acquisition

The Van der Pauw technique of sheet resistivity/Hall effect measurements was used to acquire the data for this investigation. Electrical profiling of some of the samples was done by combining the Van der Pauw technique with layer removal by etching. Measurements were made using a guarded Hall system. The measurement system consisted of four Keithley Model 610 electrometers used as unit gain amplifiers (which provided an input impedance of 10^{14} ohm), a Keithley Model 225 current source and a Systron Donner Model 7205 digital multimeter to measure sample voltages. Sample current was monitored using a Keithley Model 616 digital electrometer. Figure 1 is a diagram of the equipment configuration.

The sample to be tested was mounted on a wand type sample holder using rubber cement. Using indium solder, the sample was connected electrically to the leads on the wand which lead to the measurement system described above. For samples to be profiled, the solder and the contacts were coated with black wax that had been diluted to a paint-like consistency with trichloroethylene. This coating protected the contacts from the etchant used for layer removal during profiling. After mounting the sample on the wand the sample was placed between the poles of an electro-

magnet which could produce a magnetic field of 7600 gauss.

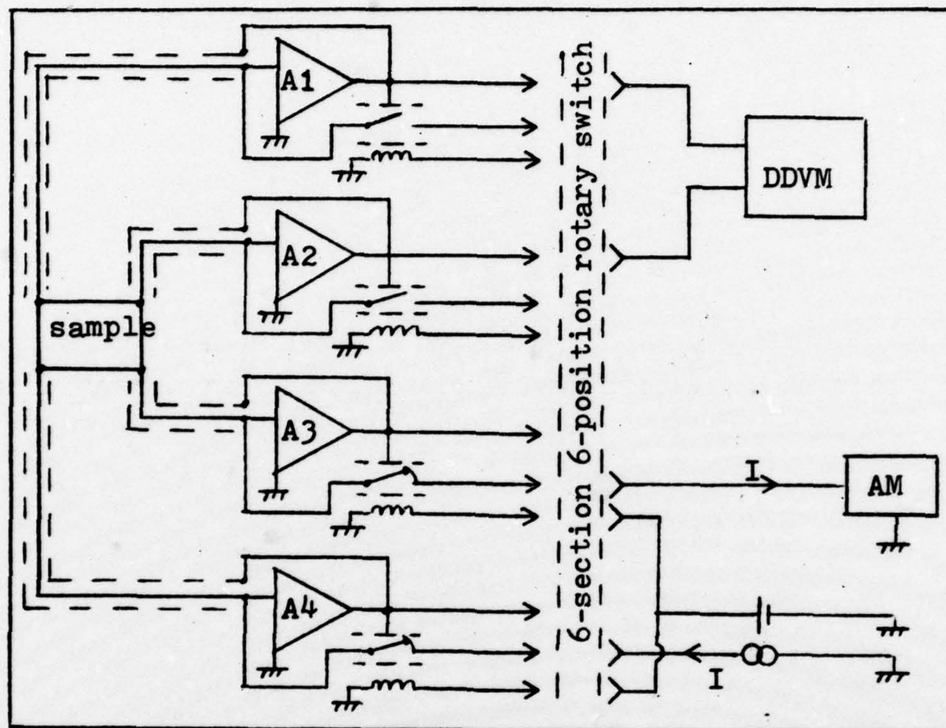

Figure 1. Van der Pauw Measurement System

The Van der Pauw technique involved measuring the voltage and current across pairs of contacts on the sample in various configurations as shown in Figure 2. The voltage and current leads were interchanged using a six-position rotary switch as shown in Figure 1. The sheet resistivity of the sample in ohms per square, was obtained from

$$\rho_s = \frac{\pi R_{avg}}{\ln 2} \qquad (2)$$

where

$$R_{avg} = \frac{R_{a1}+R_{a2}+R_{b1}+R_{b2}+R_{c1}+R_{c2}+R_{d1}+R_{d2}}{8} \qquad (3)$$

and

$$R_{a1} = \frac{V_{a1}}{I_{a1}},\ R_{a2} = \frac{V_{a2}}{I_{a2}},\ \text{etc...} \qquad (4)$$

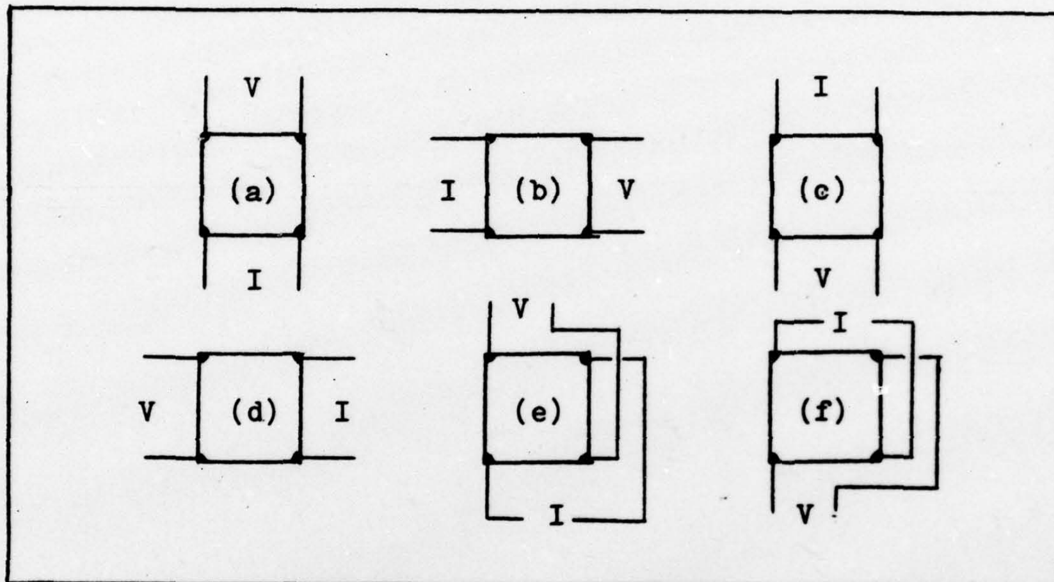

Figure 2. Sample Connections

The convention used here is that V_{a1} is the voltage measured in configuration a (see Figure 2) with a positive current applied and V_{a2} is the voltage measured with a negative current applied. The sheet Hall coefficient was obtained from

$$R_{Hs} = \frac{10^8 \Delta R_{avg}}{B} \qquad (5)$$

where B is the magnetic field strength in Gauss,

$$\Delta R_{avg} = (\Delta R_{en1}+\Delta R_{en2}+\Delta R_{er1}+\Delta R_{er2}+\Delta R_{fn1}+\Delta R_{fn2}+\Delta R_{fr1}+\Delta R_{fr2})/8 \quad (6)$$

and

$$\Delta R_{en1} = \left|\frac{V_{e1}-V_{en1}}{I_{e1}}\right|, \ \Delta R_{er2} = \left|\frac{V_{e2}-V_{er2}}{I_{e2}}\right|, \text{ etc...} \quad (7)$$

The subscripts e and f refer to the connection configuration, n and r refer to normal and reversed magnetic field directions, and 1 and 2 refer to positive and negative current, respectively. The Hall mobility and sheet carrier concentration were then found using

$$\mu_H = \frac{R_{Hs}}{\rho_s} \quad (8)$$

and

$$N_s = \frac{r}{eR_{Hs}} \quad (9)$$

where $e = 1.60219 \times 10^{-19}$ coul., the charge on an electron, and r is the ratio of Hall mobility to conduction mobility. It is generally assumed that r=1, even though use of this assumption can lead to some error in calculating N_s (Ref 17:318).

By combining layer removal with the Van der Pauw sheet resistivity/Hall effect measurements, the depth dependance of the carrier concentration and the mobility can be determined. The concentration of carriers, N_i, in the ith layer and their mobility, μ_i, can be obtained from

$$\frac{(R_s)_i}{(\rho_s^2)_i} - \frac{(R_s)_{i+1}}{(\rho_s^2)_{i+1}} = \Delta\left(\frac{R_s}{\rho_s^2}\right)_i = eN_i\mu_i^2 d_i \qquad (10)$$

and

$$1/(\rho_s)_i - 1/(\rho_s)_{i+1} = \Delta(1/\rho_s)_i = eN_i\mu_i d_i \qquad (11)$$

where $(R_s)_i$ and $(\rho_s)_i$ are the sheet Hall coefficient and the sheet resistivity measured after removal of the ith layer with thickness d_i.

Thus

$$\mu_i = \frac{\Delta(R_s/\rho_s^2)_i}{\Delta(1/\rho_s)_i} \qquad (12)$$

and

$$N_i = \frac{\Delta(1/\rho_s)_i}{ed_i\mu_i} \qquad (13)$$

These formulas were obtained from Refs 17 and 18.

Layer removal was accomplished by dipping the end of the wand with the sample mounted into the etchant, which was kept at 0^oC. The etchant consisted of a 60:1:1 solution of H_2O:30%H_2O_2:H_2SO_4 which produced etch rates of about 200 Å/min. The etch rate was measured on a quarter size sample, half covered with black wax, which was mounted on the wand along with the sample that was being measured. Successive layer removal and measurement was done until either the sample resistivity got too high or until the carrier type could not be determined. Carrier type was determined by noting the polarity of the voltage changes obtained when a magnetic field was applied to the sample.

The black wax was then removed from the quarter size sample and the resultant step measured with a Sloan Dektak microtopographer. It was assumed that the etch rate remained nearly constant each time the sample was etched. Thus the thickness of each layer removed, d_i, was found by dividing the total etch depth, measured on the quarter size sample, by the total etch time, then multiplying by the time for each etch (usually 60 or 120 sec.).

IV Experimental Results

This chapter presents the data that were collected during this investigation. The data on the Mg-implanted samples and the data on the S-implanted samples are presented separately.

Mg-implants

Electrical activation efficiencies of the Mg-implanted samples ranged from roughly 20 to 50% for an annealing temperature of 850°C. Tables II, III, and IV show the data collected for pyrolitic Si_3N_4 caps, pyrolitic SiO_2 caps and plasma Si_3N_4 caps, respectively. These tables contain the measured sheet resistance (ρ_s), mobility (μ_H), surface concentration of active carriers (N_s), and the electrical activation efficiency of each sample as a function of dose.

Table II

Pyrolitic Si_3N_4 caps -- Magnesium Implants

dose (cm^{-2})	ρ_s ($\Omega/\square$)	μ_H (cm^2/V sec)	N_s (cm^{-2})	efficiency (%)
$3x10^{12}$	$1.238x10^4$	302.9	$1.606x10^{12}$	53.52
$1x10^{13}$	3788	254.1	$6.486x10^{12}$	64.86
$5x10^{13}$	1357	212.5	$2.164x10^{13}$	43.29
$3x10^{14}$	440.6	129.4	$1.095x10^{14}$	36.50
$1x10^{15}$	345.2	113.7	$1.590x10^{14}$	15.90

Table III

Pyrolitic SiO_2 caps -- Magnesium Implants

dose (cm^{-2})	ρ_s ($\Omega/\square$)	μ_H (cm^2/V sec)	N_s (cm^{-2})	efficiency (%)
$3x10^{12}$	$2.011x10^4$	205.3	$1.512x10^{12}$	50.39
$1x10^{13}$	4551	239.7	$5.722x10^{12}$	57.22
$5x10^{13}$	1294	188.1	$2.563x10^{13}$	51.26
$3x10^{14}$	492.2	110.6	$1.146x10^{14}$	38.20
$1x10^{15}$	331.8	95.12	$1.978x10^{14}$	19.78

Table IV

Plasma Si_3N_4 caps -- Magnesium Implants

dose (cm^{-2})	ρ_s ($\Omega/\square$)	μ_H (cm^2/V sec)	N_s (cm^{-2})	efficiency (%)
$3x10^{12}$	$1.315x10^4$	287.1	$1.653x10^{12}$	55.10
$1x10^{13}$	3312	244.9	$7.696x10^{12}$	76.96
$5x10^{13}$	1008	173.0	$3.578x10^{13}$	71.56
$3x10^{14}$	412.6	127.6	$1.185x10^{14}$	39.50
$1x10^{15}$	319.6	108.9	$1.793x10^{14}$	17.93

Some general trends can be observed in the data. For all three encapsulants, it was observed that the sheet resistance decreased with increasing dose. This was expected, since the sheet resistance of a sample is directly related to the number of active carriers in the implanted layer. The mobilities also generally decreased with increasing dose. This was also expected, since for higher doses there are more impurities to scatter the active carriers, thus decreasing the mobility. Also, as expected, the measured surface carrier concentrations increased with increasing dose. The electrical activation efficiencies generally decreased with increasing dose, in accordance with previously reported results (Refs 4, 5, 7, 14, 15, 22)

There were, however, a few exceptions to these general trends. For the pyrolitic Si_3N_4 encapsulant, the electrical activation efficiency measured for a dose of $1x10^{13}cm^{-2}$ was higher than that measured for a dose of $3x10^{12}cm^{-2}$ (see Table II). For the pyrolitic SiO_2 encapsulant, both the electrical activation efficiency and the mobility were higher for the sample implanted with a dose of $1x10^{13}cm^{-2}$ than those for a dose of $3x10^{12}cm^{-2}$ (see Table III). For the plasma Si_3N_4 encapsulant, the electrical activation efficiency was also higher for a dose of $1x10^{13}cm^{-2}$ than for a dose of $3x10^{12}cm^{-2}$ (see Table IV). This data suggests that the highest electrical activation efficiency can be achieved for a dose around $1x10^{13}cm^{-2}$, efficiency decreasing for both higher and lower doses.

Table V

Electrical Activation Efficiencies (%) for

Different Encapsulants -- Magnesium Implants

dose (cm^{-3})	pyrolitic Si_3N_4	pyrolitic SiO_2	plasma Si_3N_4
$3x10^{12}$	53.52	50.39	55.10
$1x10^{13}$	64.86	57.22	76.96
$5x10^{13}$	43.29	51.26	71.56
$3x10^{14}$	36.50	38.20	39.50
$1x10^{15}$	15.90	19.78	17.93

As previously stated, the purpose of this study was to compare the effectiveness of different encapsulants. Thus the electrical activation efficiencies of the Mg-implanted samples were retabulated in Table V to facilitate their comparison. Table V shows that the activation of the plasma Si_3N_4 capped samples was consistently higher than the activation of samples capped with the other two encapsulants, for doses less than $1x10^{15}cm^{-2}$. The differences in the electrical activations for the three encapsulants are generally not very large, however. This fact is shown graphically in Figure 3 which shows the surface concentration of active carriers and their mobility as a function of dose. The curves for the three encapsulants all show the same trends and are quite close to each other. The

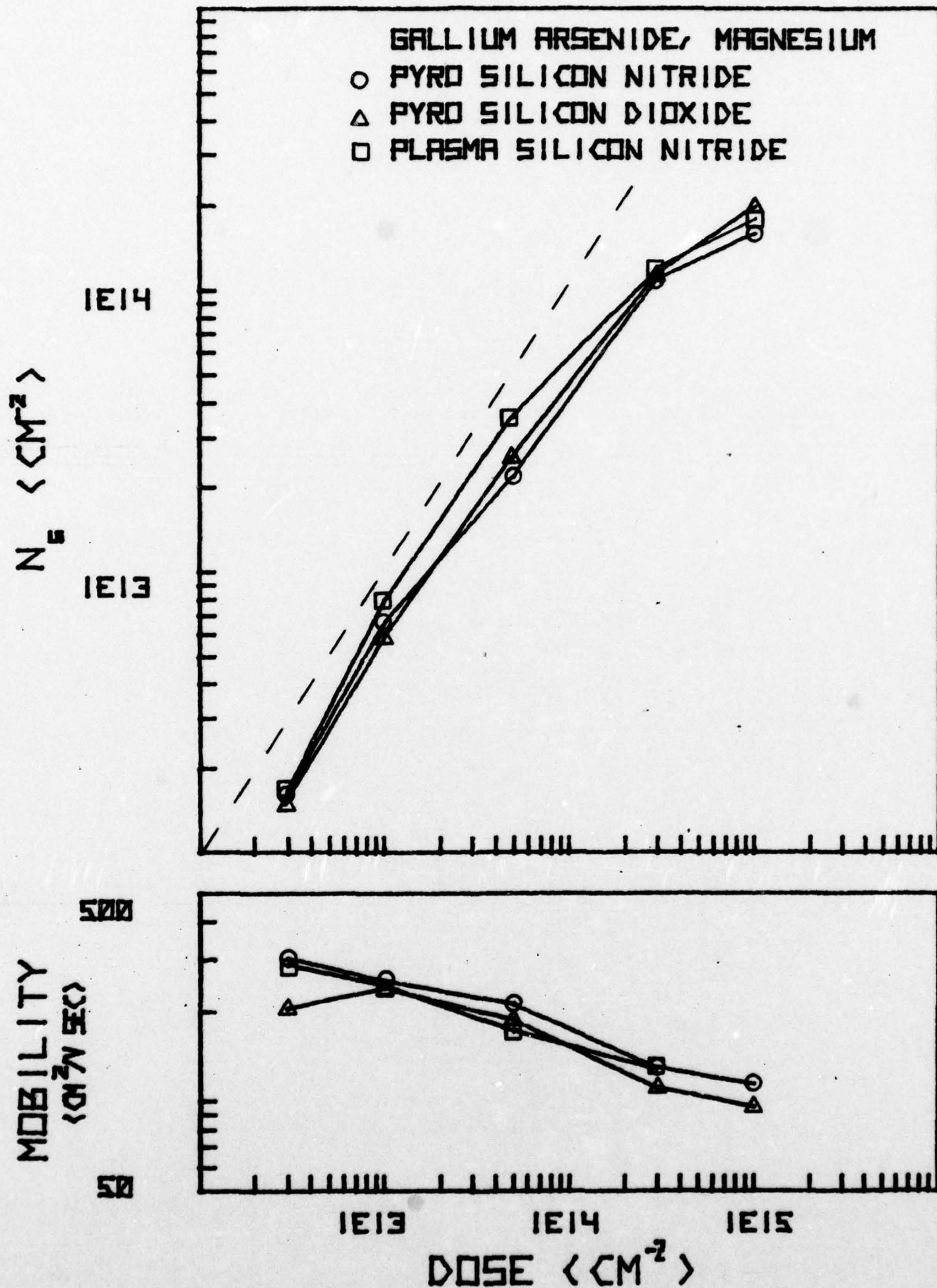

Figure 3. Surface Concentration and Mobility as Functions of Dose

dashed line in the upper plot of Figure 3 represents 100% electrical activation of the implanted ions.

In addition to the electrical activation measurements, carrier concentration and mobility versus depth profiles were measured for some of the samples. In particular, Mg-implanted samples with doses of $5x10^{13}$ and $3x10^{14}cm^{-2}$ were profiled, using the Van der Pauw technique described in Chapter III. The profile for the sample implanted with $5x10^{13}$ mg ions cm^{-2} and capped with pyrolitic Si_3N_4 is shown in Figure 4. The profiles for the other encapsulants are contained in Appendix A (Figures 9 and 10). The solid, parobolic-shaped curve on all the profile plots is the LSS-predicted carrier concentration distribution profile.

The electrical profiles obtained using the different encapsulants on samples implanted with a dose of $5x10^{13}cm^{-2}$ are compared in Figure 5. The measured distributions extend to roughly 2.5 times the LSS projected range (the depth of the peak of the LSS profile). This is believed to be largely due to diffusion during annealing. The resulting profiles are approximately uniform, without a clearly defined peak. Figure 5 also illustrates that using the plasma Si_3N_4 cap resulted in higher concentrations of active carriers. The pyrolitic Si_3N_4- and SiO_2- capped samples exhibited very similar profiles, except near the surface where the pyrolitic SiO_2- capped sample had a higher concentration. The mobility profiles of all three samples are

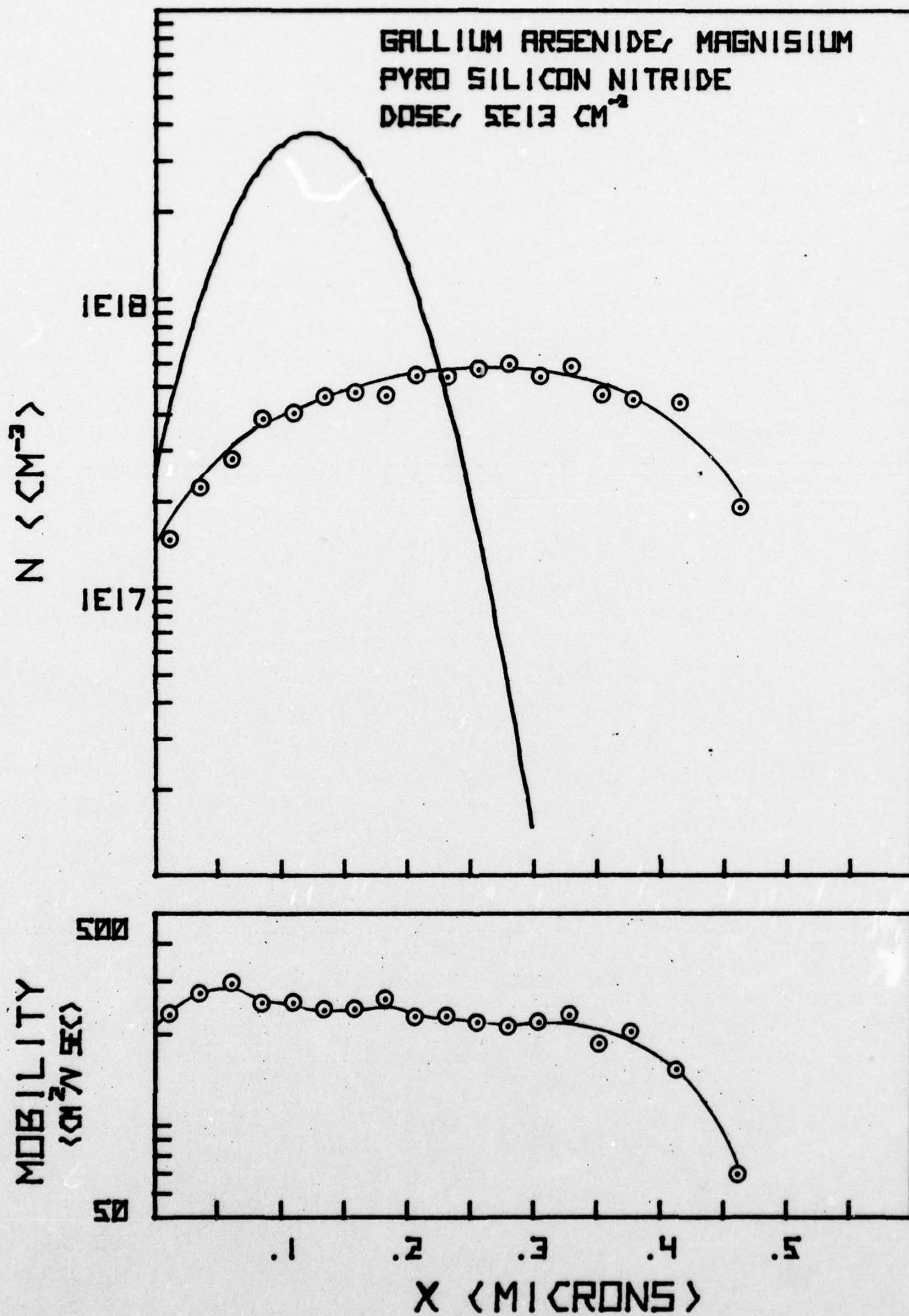

Figure 4. Carrier Concentration and Mobility Profile

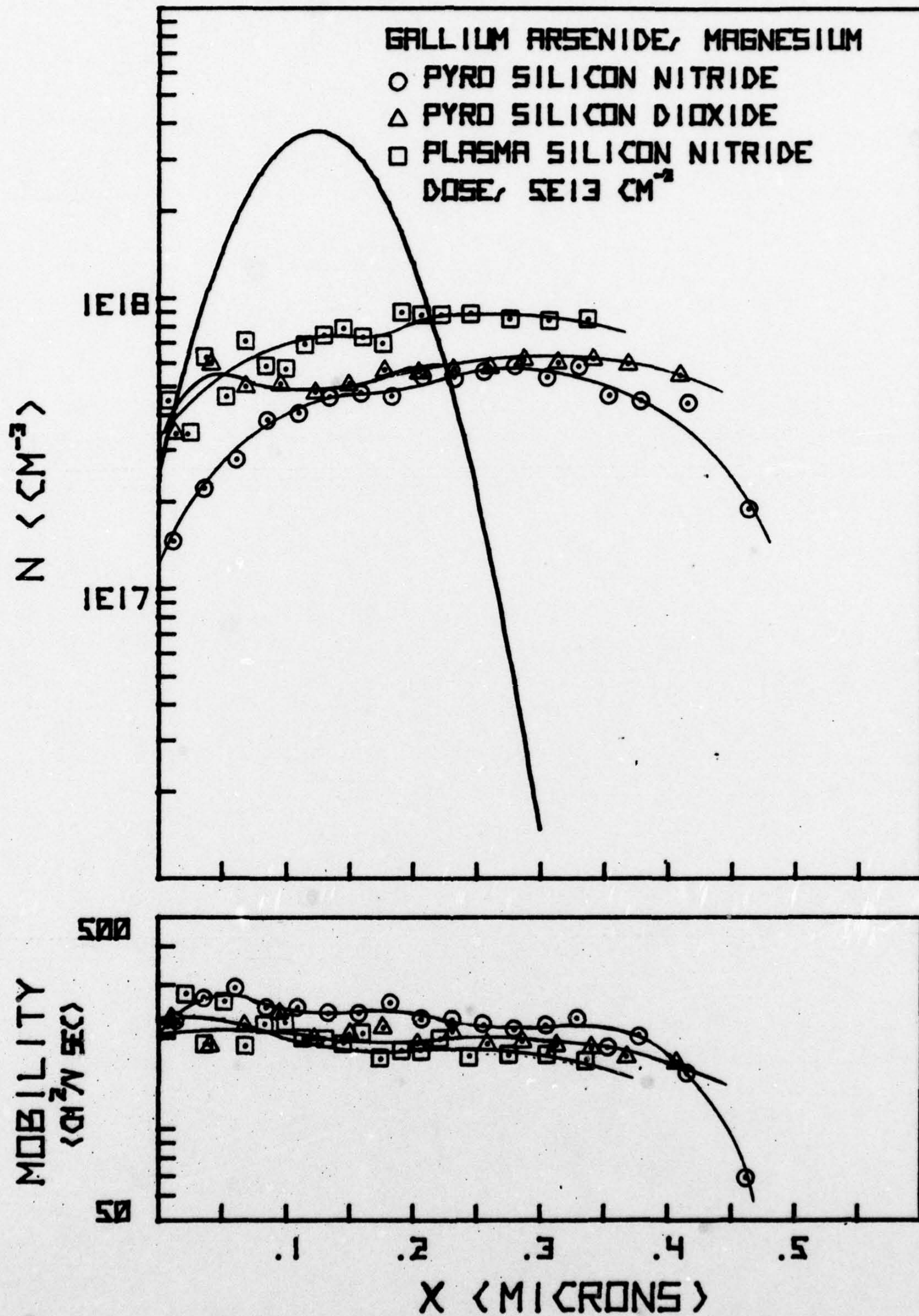

Figure 5. Electrical Profile Comparison for Different Encapsulants

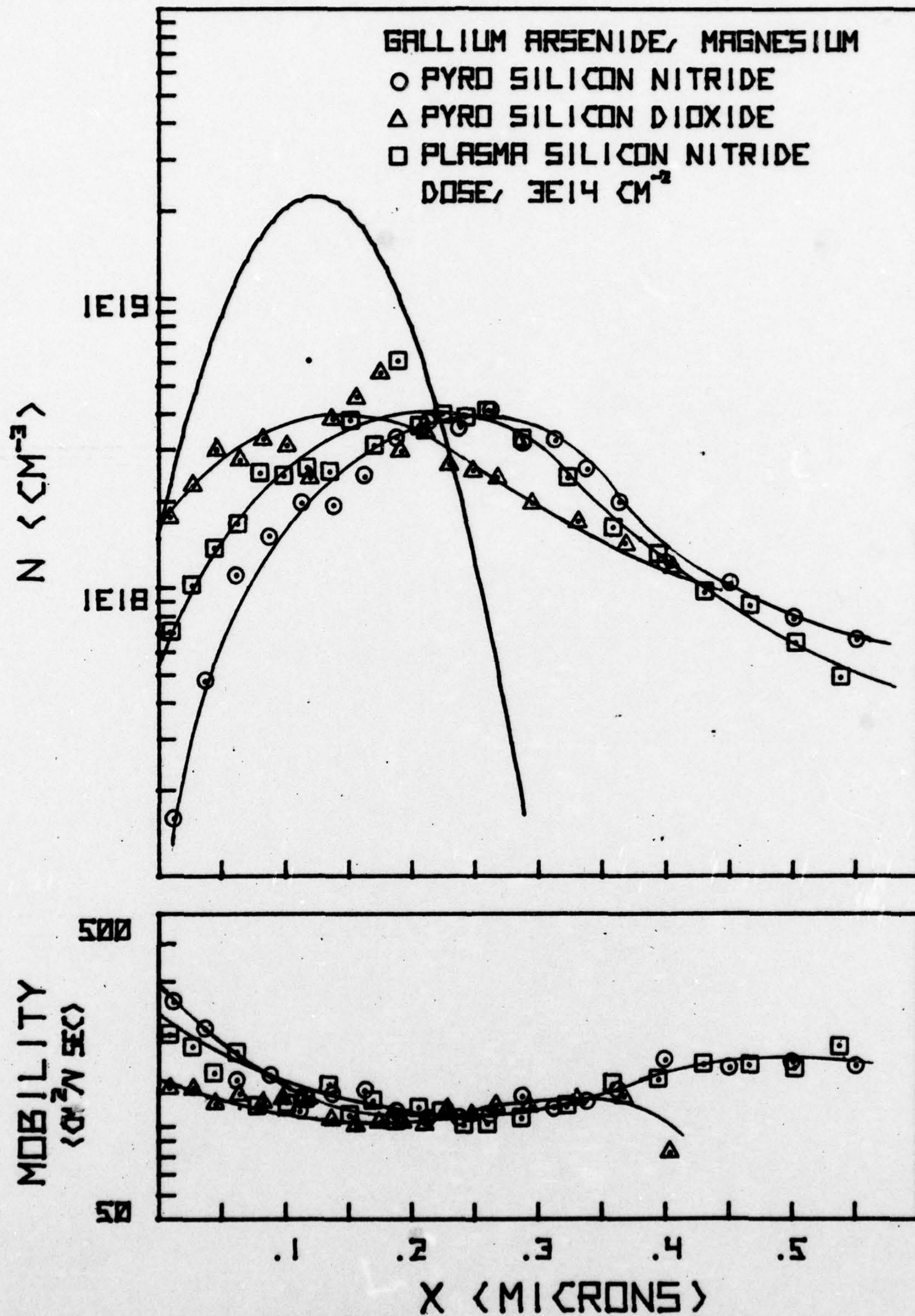

Figure 6. Electrical Profile Comparison for Different Encapsulants

close together, all showing decreasing values of mobility with increasing depth (X).

The electrical profiles obtained using the different encapsulants on samples implanted with a dose of $3x10^{14}cm^{-2}$ are compared in Figure 6. The profiles for the individual samples are given in Appendix A, Figures 11, 12, and 13. These profiles show a peak value of about $3x10^{18}cm^{-3}$ which is, in all cases, deeper than the LSS prediction. Again this is probably due to diffusion during annealing. At this dose the three encapsulants produced concentration profiles with identifiable peaks at different depths. The pyrolitic SiO_2- capped sample exhibited the shallowest peak, and the pyrolitic Si_3N_4- capped sample exhibited the deepest peak. The mobility profiles show decreased mobility near the peaks of concentration profiles, as expected.

S-Implants

The electrical activation efficiencies of the S-implanted samples ranged from roughly 5 to 40%, in general significantly lower than for Mg-implanted samples. This agrees with previous works showing activation for p-type implants usually higher than activation for n-type implants (Ref 23). Tables VI, VII, and VIII show the data collected from the S-implanted samples for pyrolitic Si_3N_4 caps, pyrolitic SiO_2 caps, and plasma Si_3N_4 caps respectively.

The same general trends are evident in these data as observed in the data for the Mg-implanted samples. These

trends are that sheet resistance, mobility, and electrical activation efficiency decreased, and the measured surface carrier concentrations increased with increasing dose. However, exceptions to these trends were also evident. For the pyrolitic Si_3N_4 caps the sheet resistance measured for a dose of $1x10^{14}cm^{-2}$ was higher than that measured for a dose of $3x10^{13}cm^{-2}$, and the mobility measured for a dose of $3x10^{14}cm^{-2}$ was higher than that measured for a dose of $1x10^{14}cm^{-2}$ (see Table VI). For the pyrolitic SiO_2 caps, the sheet resistance measured for a dose of $3x10^{13}cm^{-2}$ was unusually low compared with those measured for higher doses (see Table VII). The same phenomena was observed with the plasma Si_3N_4 caps. For all the encapsulants studied, the electrical activation efficiencies increased for a dose of $3x10^{13}cm^{-2}$ then very sharply decreased for higher doses.

Table VI

Pyrolitic Si_3N_4 caps -- Sulfur Implants

dose (cm^{-2})	ρ_s ($\Omega/\square$)	μ_H (cm^2/V sec)	N_s (cm^{-2})	efficiency (%)
$3x10^{12}$	1548	3953	$1.020x10^{12}$	34.01
$1x10^{13}$	698.8	3700	$2.414x10^{12}$	24.14
$3x10^{13}$	174.2	3302	$1.085x10^{13}$	36.17
$1x10^{14}$	353.5	2792	$6.323x10^{12}$	6.323
$3x10^{14}$	224.9	3034	$9.150x10^{12}$	3.050

Table VII

Pyrolitic SiO_2 caps -- Sulfur Implants

dose (cm^{-2})	ρ_s ($\Omega/\square$)	μ_H ($cm^2/V\ sec$)	N_s (cm^{-2})	efficiency (%)
$3x10^{12}$	**	**	**	**
$1x10^{13}$	609.1	3676	$2.787x10^{12}$	27.87
$3x10^{13}$	144.2	3431	$1.262x10^{13}$	42.06
$1x10^{14}$	345.0	2871	$6.301x10^{12}$	6.301
$3x10^{14}$	324.0	2810	$6.851x10^{12}$	2.184

Table VIII

Plasma Si_3N_4 caps -- Sulfur Implants

dose (cm^{-2})	ρ_s ($\Omega/\square$)	μ_H ($cm^2/V\ sec$)	N_s (cm^{-2})	efficiency (%)
*$3x10^{12}$	1914	4687	$6.957x10^{11}$	23.19
$1x10^{13}$	**	**	**	**
$3x10^{13}$	146.2	3172	$1.346x10^{13}$	44.88
$1x10^{14}$	234.6	2482	$1.072x10^{13}$	10.72
$3x10^{14}$	**	**	**	**

* data for this sample was marginal
** no data available

Table IX

Electrical Activation Efficiencies (%) for

Different Encapsulants -- Sulfur Implants

dose (cm^{-2})	pyrolitic Si_3N_4	pyrolitic SiO_2	plasma Si_3N_4
$3x10^{12}$	34.01	**	23.19
$1x10^{13}$	24.14	27.87	**
$3x10^{13}$	36.17	42.06	44.38
$1x10^{14}$	6.323	6.301	10.72
$3x10^{14}$	3.050	2.284	**

To aid in their comparison, the electrical activation efficiencies of the S-implanted samples were retabulated in Table IX. Table IX shows that, where good data were available for all three encapsulants, the plasma Si_3N_4 caps produced the highest activations. The pyrolitic SiO_2 caps produced nearly equal or higher activation than the pyrolitic Si_3N_4 caps. As with the Mg-implanted samples, the differences in activations for the different encapsulants are not very large. The largest difference was between the plasma Si_3N_4 cap and the pyrolitic SiO_2 cap for a dose of $1x10^{14}cm^{-2}$, the activations differing by a factor of 1.7. These small differences in electrical activation efficiencies between encapsulants are illustrated in Figure 7, which shows the surface concentration of active carriers and their mobility as a function of dose. The surface concentration of active carriers is highest for a dose of $3x10^{13}cm^{-2}$ then

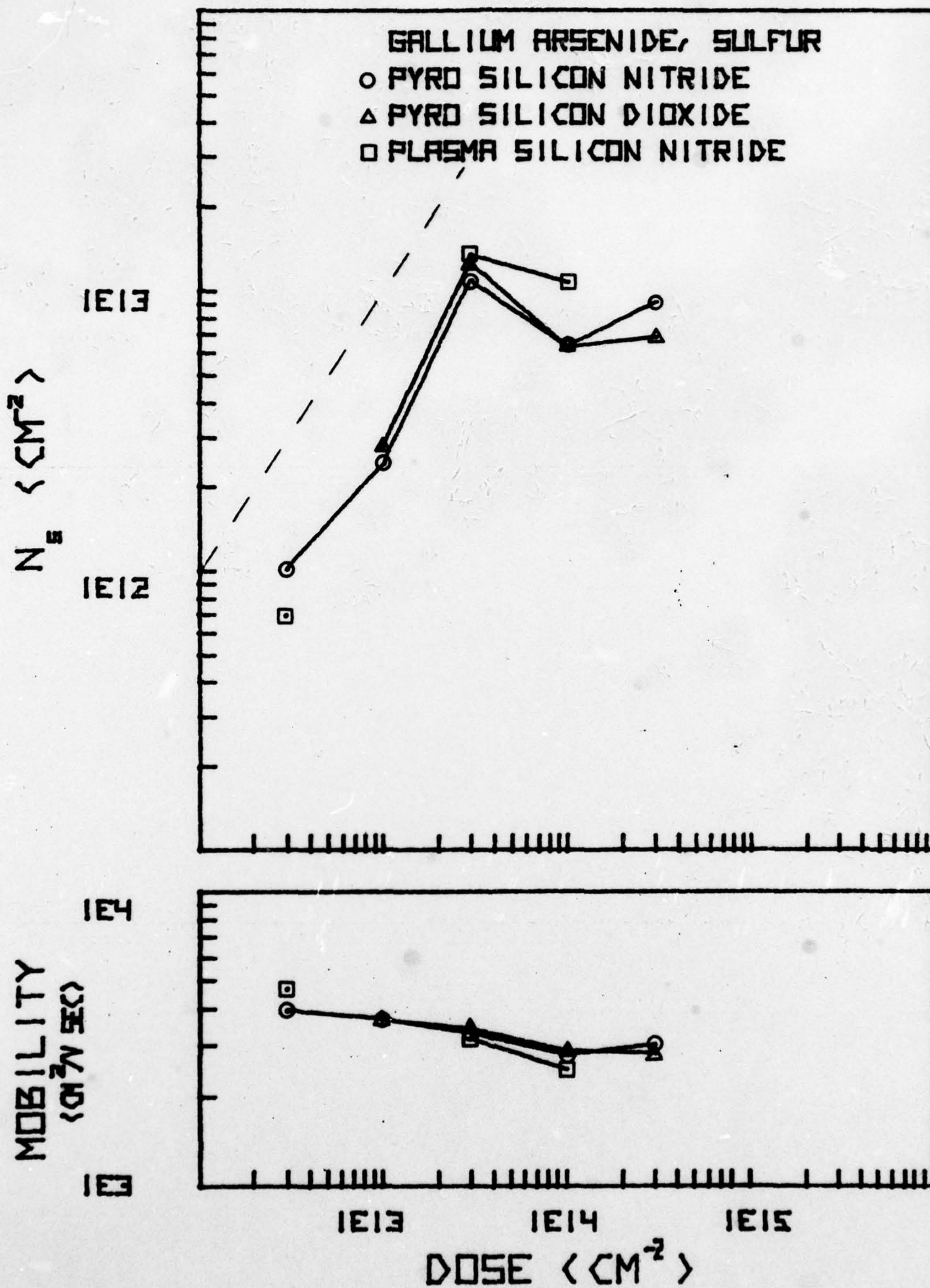

Figure 7. Surface Concentration and Mobility as Functions of Dose

drops and levels off to about $7\times10^{12}cm^{-2}$ for higher doses, indicating a saturation condition. It should be noted that the samples implanted with the two higher doses came from a different substrate than the samples implanted with the three lower doses. This may partially account for the sudden drop in efficiency observed in Figure 7. Figure 7 also shows the mobilities for all three encapsulants generally decreasing with increasing dose, as previously noted.

Carrier concentration and mobility profiles were also measured for the S-implanted samples. In particular, the samples implanted with a dose of $3\times10^{13}cm^{-2}$ were profiled. The profiles measured for samples with three different encapsulants are presented in Appendix A, Figures 14, 15, and 16. Figure 8 shows all three profiles on one plot for comparison. The samples capped with pyrolitic Si_3N_4 and pyrolitic SiO_2 exhibited nearly identical profiles, with peak concentrations of $6\times10^{17}cm^{-3}$. The sample capped with plasma Si_3N_4 had a peak concentration sightly higher than $1\times10^{18}cm^{-3}$. For all three encapsulants, the peaks in the carrier concentration profiles were shallower than the peak of the LSS-predicted profile. The mobility profiles for the three samples were very close together.

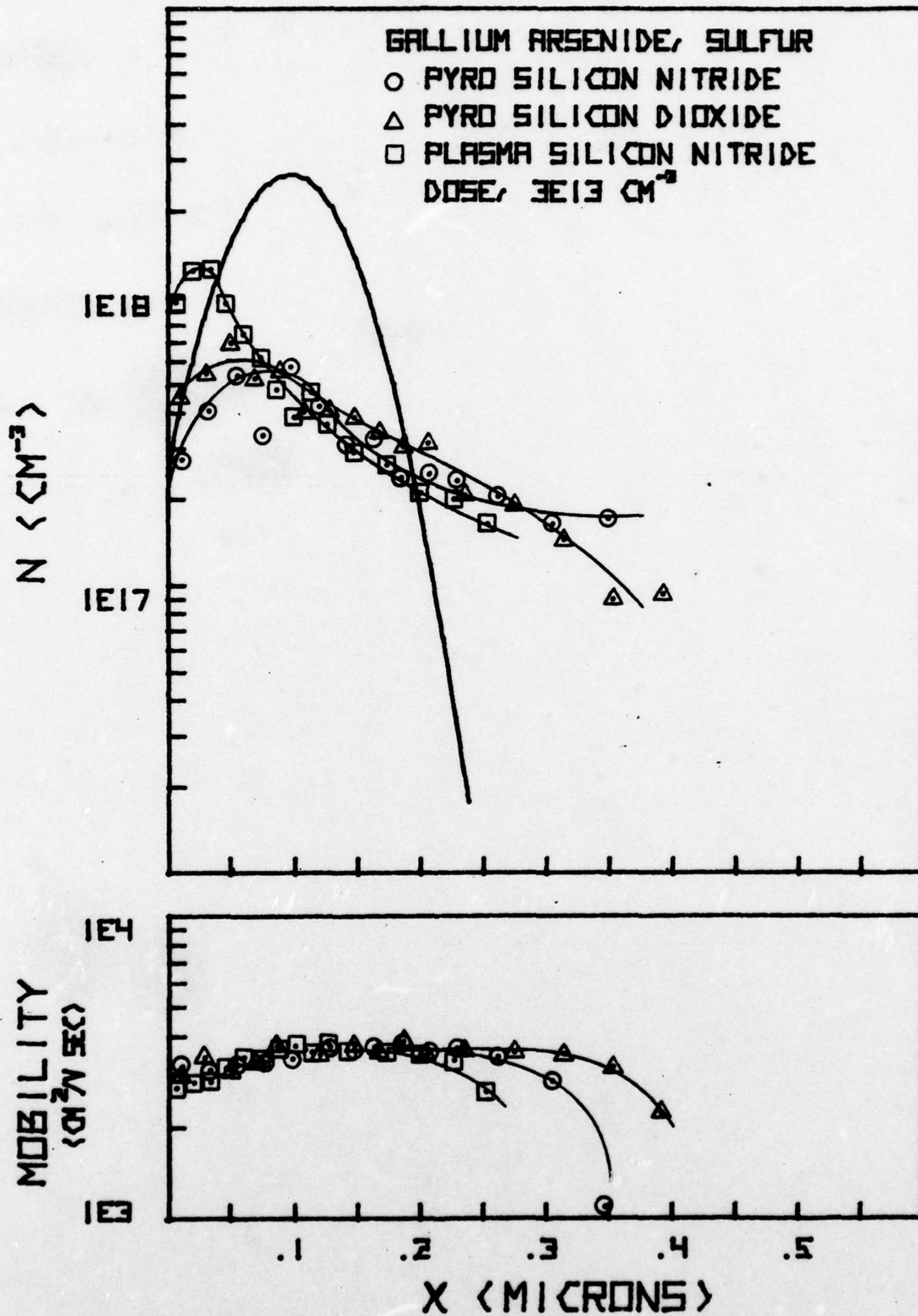

Figure 8. Electrical Profile Comparison for Different Encapsulants

V Discussion of Experimental Results

Only the measurements for one sample per set of conditions (implant species, dose, and cap) were collected, because of time limitations. Thus the results as presented have not been confirmed by a number of repeated runs.

The three encapsulants studied produced very similar results, as far as electrical measurements are concerned, for both Mg (p-type) and S (n-type) implants. The electrical activation efficiencies were found to be highly dose dependent. But, for any given dose, the differences between the activations produced by the different encapsulants were not very great. For the Mg-implants, the largest difference in activations for different encapsulants was observed for a dose of $5\times10^{13}cm^{-2}$ between the plasma Si_3N_4 and the pyrolitic Si_3N_4 encapsulants. Their activations differed by a factor of 1.7. For the S-implants, the largest difference in activations for different encapsulants was observed for a dose of $1\times10^{14}cm^{-2}$ between the plasma Si_3N_4 and the pyrolitic SiO_2 encapsulants. Their activations also differed by a factor of 1.7. On the average, the electrical activation efficiencies for a given dose differed by a factor of 1.2 for Mg-implants and 1.3 for S-implants.

In addition to similar activation measurements, samples capped with the three different encapsulants exhibited very similar electrical profiles. This was shown by Fig-

ures 5 and 6 for the Mg-implants and by Figure 8 for the S-implants. The peaks in the electrical profiles of the Mg-implanted samples were deeper than predicted by LSS theory. This was expected, however, because of diffusion during the annealing process. The peaks in the electrical profiles of the S-implanted samples were slightly shallower than predicted by LSS theory. Other workers, such as Welch et al. (Ref 19), and Woodcock et al. (Ref 20) have reported electrical profiles of S-implants which extend much deeper than those predicted by LSS theory.

Although the plasma Si_3N_4 encapsulants produced higher electrical activations, as pointed out in Chapter IV, they did not hold up to the annealing process as well as the other encapsulants. Several samples that were capped with plasma Si_3N_4 had to be discarded because they pitted during the annealing process. Wherever pits occured in the cap, there were also pits in the surface of the sample due to the decomposition of the GaAs.

It should be pointed out that while this investigation was in progress, the plasma capping procedure was still being "fine tuned" to achieve better caps. Most of the caps used in this study were made before the following changes in the plasma capping system were made. The silane source was changed from a 5% mixture with N_2 to a 2% mixture with Ar so that better control of the silane flow could be achieved. A thermocouple was added to the plate holding the samples. Before, the deposition temperature was measured at the heat-

er on which the sample holder was placed. A temperature difference of about 100°C was found between the heater and the sample holder temperature. After the addition of the thermocouple, it was found that a deposition temperature of 150°C gave best results.

As a whole, the results of this study were consistent with previous investigations. All of the previous studies which compared SiO_2 to Si_3N_4 encapsulants (for n-type implants) found Si_3N_4 to be superior. In this study, the plasma Si_3N_4 caps produced the highest activations for all doses. However, in some cases the pyrolitic SiO_2 caps produced higher activations than the pyrolitic Si_3N_4 caps.

Davies, et al. (Ref 8) studied different encapsulants for group IV (S and Se) and group VI (Si) n-type implants. They found that low activation of the group IV implants was produced by the SiO_2 caps because of Ga outdiffusion. The Ga vacancies thus produced acted as compensation centers for the group IV implants which occupied arsenic sites. This was confirmed by adding Ga to the SiO_2 cap, which decreased the Ga outdiffusion and increased the activation.

However, adding Ga to SiO_2 caps decreased the activations of the group VI implants, since they occupied gallium sites. Si_3N_4 caps were also shown to prevent Ga outdiffusion. Following their reasoning, SiO_2 caps should also be superior for group II (p-type) implants, which also occupy gallium sites. Summarizing, because Ga outdiffusion is greater for SiO_2 caps than for Si_3N_4 caps, the former should

be superior for p-type dopants (which occupy Ga vacancies) and the latter for n-type dopants (for which Ga vacancies serve as compensation complexes). The results of this investigation do not support this hypothesis. For Mg-implanted samples (p-type), Si_3N_4 caps (both pyrolitic and plasma) produced nearly equal or higher activations than SiO_2 caps. For S-implanted samples (n-type) pyrolitic SiO_2 caps produced nearly equal or higher activations than pyrolitic Si_3N_4 caps.

VI. Summary and Recommendations

The purpose of this investigation was to study the electrical effects of pyrolitic Si_3N_4, SiO_2, and plasma deposited Si_3N_4 encapsulants on ion implanted GaAs. It was shown that there was not a great deal of difference in the observed electrical activation efficiencies produced when the three different encapsulants are used. For the Mg-implanted samples, plasma Si_3N_4 encapsulated samples exhibited the highest electrical activations for all doses except $1x10^{15}$ cm^{-2}. S-implanted samples that were capped with plasma Si_3N_4 also exhibited the highest electrical activations.

Both Mg-implanted and S-implanted samples exhibited very similar electrical profiles for the different encapsulants. However, the observed peak in the profiles for the S-implanted samples was closer to the surface than what LSS theory predicted, while the peak in the profiles for the Mg-implanted samples was deeper than predicted by LSS (which can be accounted for by diffusion during annealing).

Previous investigations had shown that because Ga outdiffusion was greater for SiO_2 caps than Si_3N_4 caps, the former would be superior for p-type dopants and the latter for n-type dopants. However, in this study, the activations observed for Mg-implanted (p-type) samples with Si_3N_4 caps was generally nearly equal to or greater than the activation

observed with SiO_2 caps. The activation observed for S-implanted (n-type) samples with SiO_2 caps was generally equal to or greater than the activation observed with pyrolitic Si_3N_4 caps. (But, activations were higher still with plasma Si_3N_4 caps.)

It was generally shown that, of the three encapsulants studied, the plasma Si_3N_4 encapsulants seemed to be the better encapsulant for both S and Mg implants. Further investigation could be done along the lines of determining the annealing temperature range over which the encapsulants are reliable (this study only used an annealing temperature of 850°C). This investigation should be repeated with different n- and p-type implants to determine if the reported results are repeatable.

Effective encapsulants, producing high electrical activations in implanted layers, are very important to device fabrication in GaAs. Thus, future studies aimed at determining the best encapsulant for annealing different implants in GaAs will always be very important.

Bibliography

1. Baron, R., G. A. Shifrin, O. J. Marsh, and J. W. Mayer. "Electrical behavior of Group III and Group V implanted dopants in Si," Journal of Applied Physics, 40: 3702-3719, no. 9, August 1969.

2. Pashley, R. D., J. W. Mayer, F. H. Eisen, and B.Welch. "Comparison of encapsulating dielectrics on ion implanted GaAs," Electrochemical Society Journal, 121: 99c, no. 3, March 1974.

3. Bell, E. C., A. E. Glaccum, P. L. F. Hemment, and B. J. Sealy. "Heat treatment of ion implanted GaAs," Radiation Effects, 22: 253-258, no 4, August 1974.

4. Sealy, B. J., and R. K. Surridge. "A new thin film encapsulant for ion implanted GaAs," Thin Solid Films, 26: L19-22, no. 2, April 1975.

5. Donnelly, J. P., W. T. Lindley, and C. E. Hurwitz. "Silicon- and selenium-ion implanted GaAs reproducibly annealed at temperatures up to 950°C," Applied Physics Letters, 27: 41-43, no. 1, 1 July 1975.

6. Sealy, B.J., and A. E. D'Cruz. "Encapsulation of ion-implanted GaAs using native oxides," Electronic Letters, 11: 323-324, no. 15, 14 July 1975.

7. Pashley, R. D. "Tellurium-implanted n^+ layers in GaAs," Solid State Electronics, 18: 977-981, no. 11, November 1975.

8. Davies, D. E., J. K. Kennedy, and C. E. Ludington. "Comparison of group IV and VI doping by implantation in GaAs," Electrochemical Society Journal, 122: 1374-1377, no. 19, October 1975.

9. Sealy, B. J., and J. M. Ritchie. "A comparison of SiO_2 and Si_3N_4 coatings on GaAs using transmission electron microscopy," Thin Solid Films, 35: 127-130, June 1976.

10. Immorlica, A. A., and F. H. Eisen. "Capless annealing of ion-implanted GaAs," Applied Physics Letters, 29: 94-5, no. 2, 15 July 1976.

11. Malbon, R. M., D. H. Lee, and J. M. Whelan. "Annealing of ion-implanted GaAs in a controlled atmosphere," Electrochemical Society Journal, 123: 1413-5, no. 9, September 1976.

12. Eisen, F. H., and B. M. Welch. "Tellurium implantation in GaAs," *Solid State Electronics*, 20: 219-23, no. 3, March 1977.

13. Donnelly, J. P., C. O. Bozlen, and W. T. Lindley. "Low dose n-type ion implantation into Cr- doped GaAs substrates," *Solid State Electronics*, 20: 273-6, no. 3, March 1977.

14. Gamo, K., T. Inada, S. Krekler, J. W. Mayer, F. H. Eisen, and B. M. Welch. "Selenium implantation in GaAs," *Solid State Electronics*, 20: 213-7, no. 3, March 1977.

15. Lidlow,A., J. F. Gibbons, and T. Magee. "A double-layered encapsulant for annealing ion-implanted GaAs up to 1100°C," *Applied Physics Letters*, 31: 158-61, no. 3, 1 August 1977.

16. Lyons, R. P., Jr., *Ion Implantation of Diatomic Sulfur into GaAs*. Unpublished thesis. Wright-Patterson Air Force Base, Ohio: Air Force Institute of Technology, September 1974.

17. Johansson, N. G. E., J. W. Mayer, and O. J. Marsh. "Technique used in Hall effect analysis of ion implanted Si and Ge," *Solid State Electronics*, 13: 317-35, 1970.

18. Van der Pauw, L. J. "A method of measuring the resistivity and Hall coefficient on lamellae of arbitrary shape," *Phillips Technical Review*, 20: 220-224, 1958.

19. Welch, B. M., F. H. Eisen, and J. A. Higgins. "GaAs field-effect transistors by ion implantation," *Journal of Applied Physics*, 45: 3685-7, August 1974.

20. Woodcock, J. M., J. M. Shannon, and D. J. Clark. "Electrical and cathodoluminescence measurements on ion implanted donor layers in GaAs," *Solid State Electronics*, 18: 267-75, March 1975.

21. Gibbons, J. F., et al. *Projected Range Statistics*. Stroudsburg: Dowden, Hutchinson and Ross, Inc.

22. Yeo, Y. K., T. S. Park, and P. W. Yu. "Electrical measurements and optical activation studies in Mg-implanted GaAs," to be published.

23. Eisen, F. H., "Ion implantation in III-V compounds," Ion Implantation in Semiconductors, Science and Technology. Plenum Press, N.Y., 1975.

Appendix A

Other Electrical Profiles

These profiles are part of the results referenced by Chapter IV.

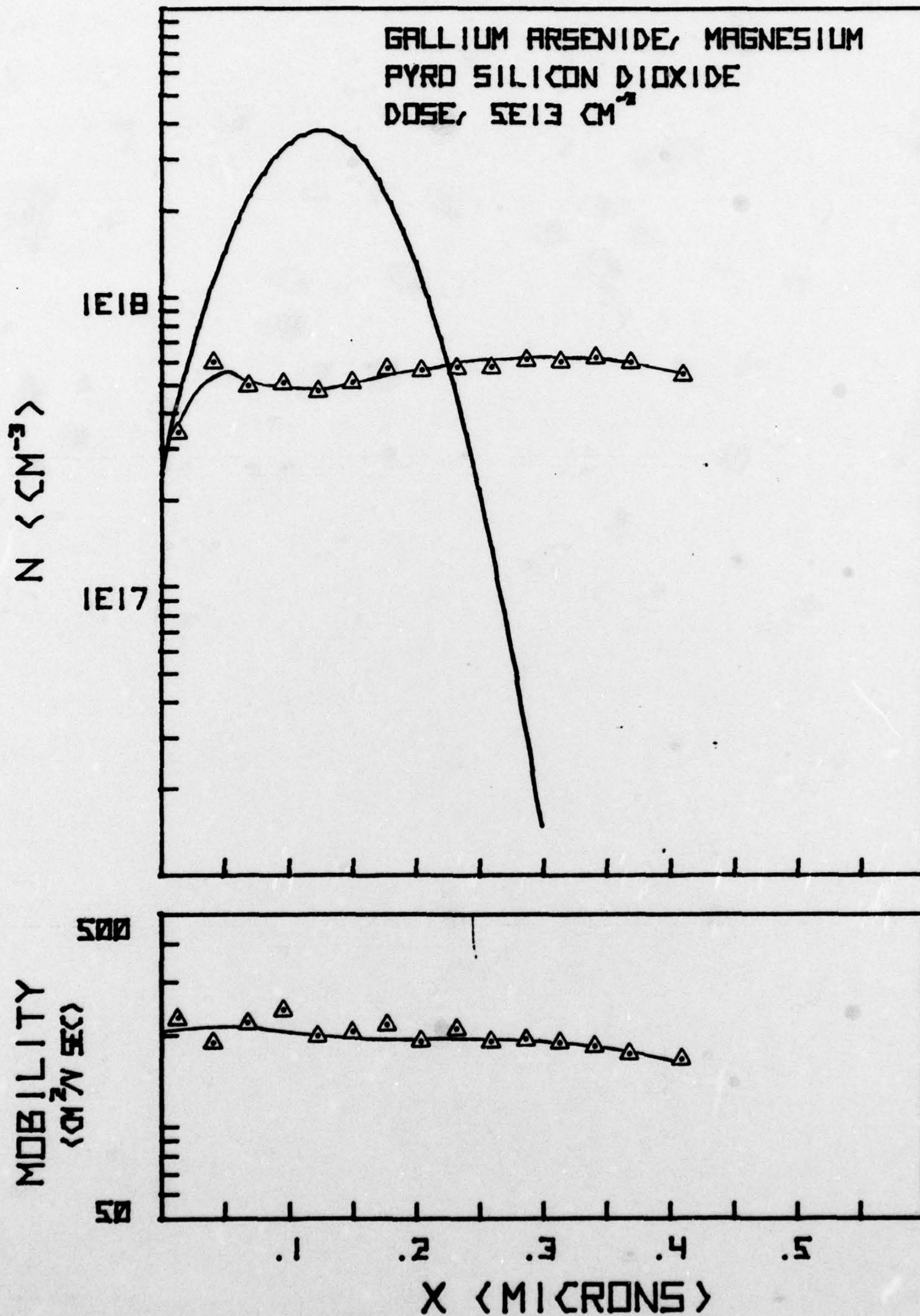

Figure 9. Carrier Concentration and Mobility Profile

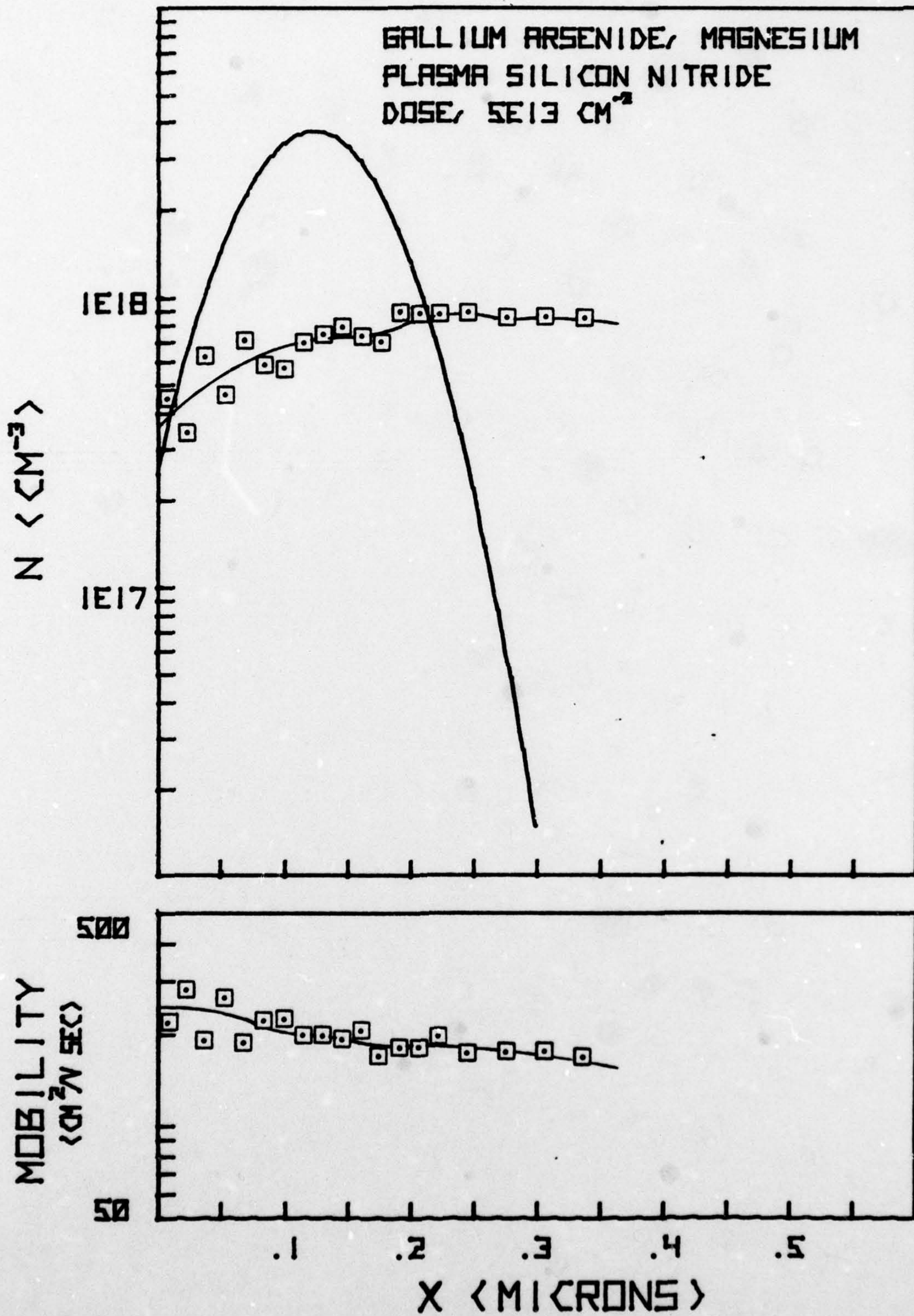

Figure 10. Carrier Concentration and Mobility Profile

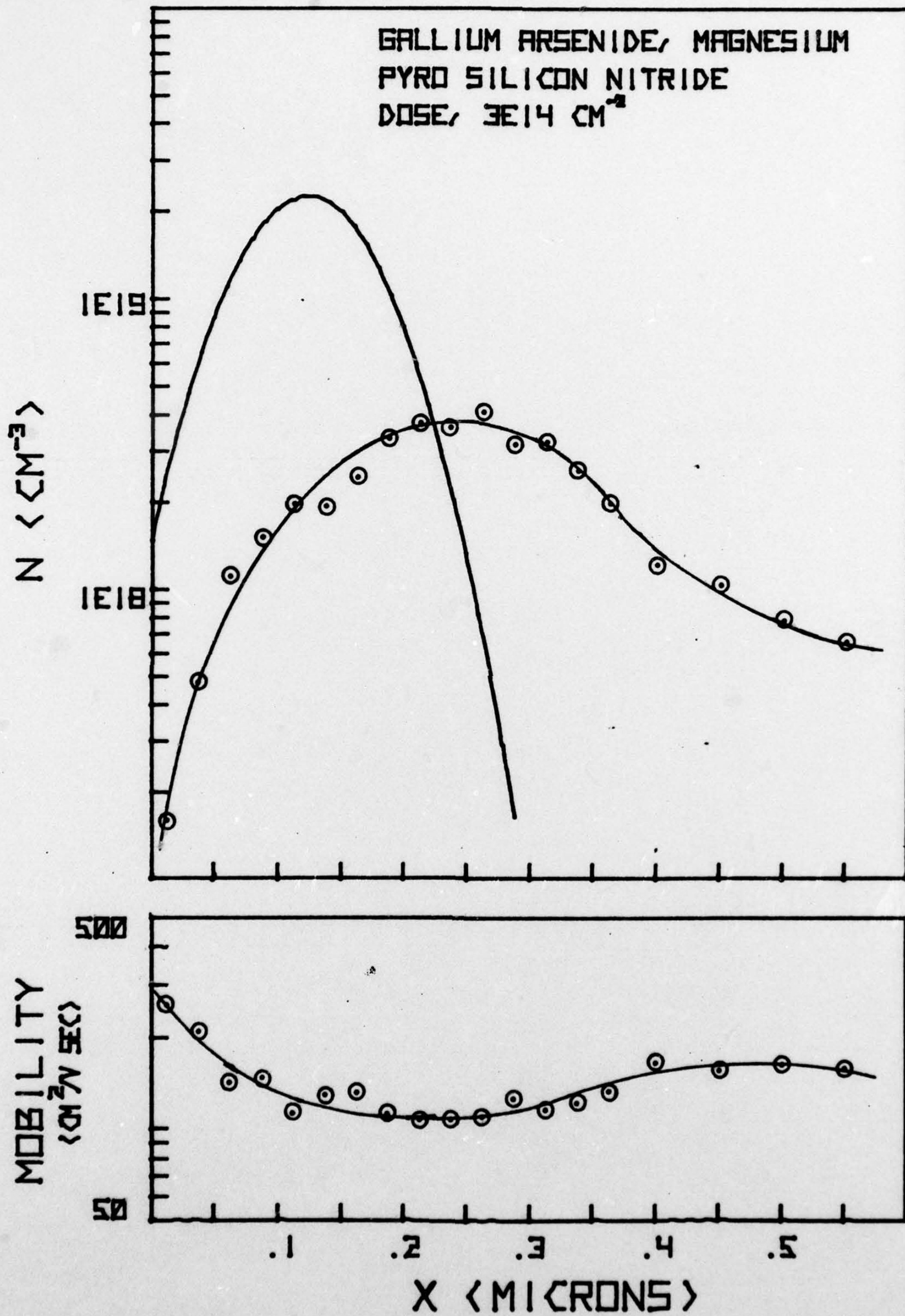

Figure 11. Carrier Concentration and Mobility Profile

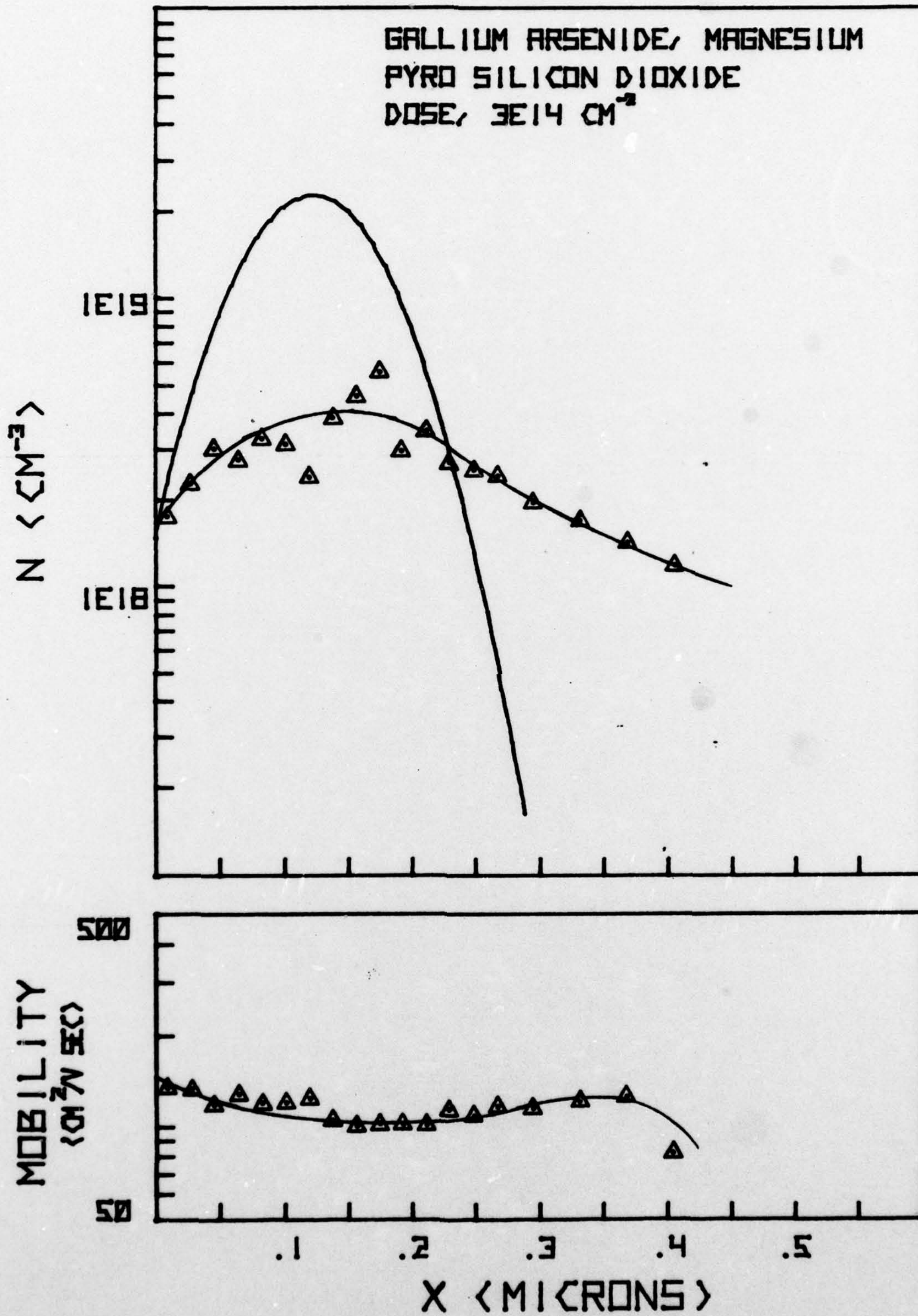

Figure 12. Carrier Concentration and Mobility Profile

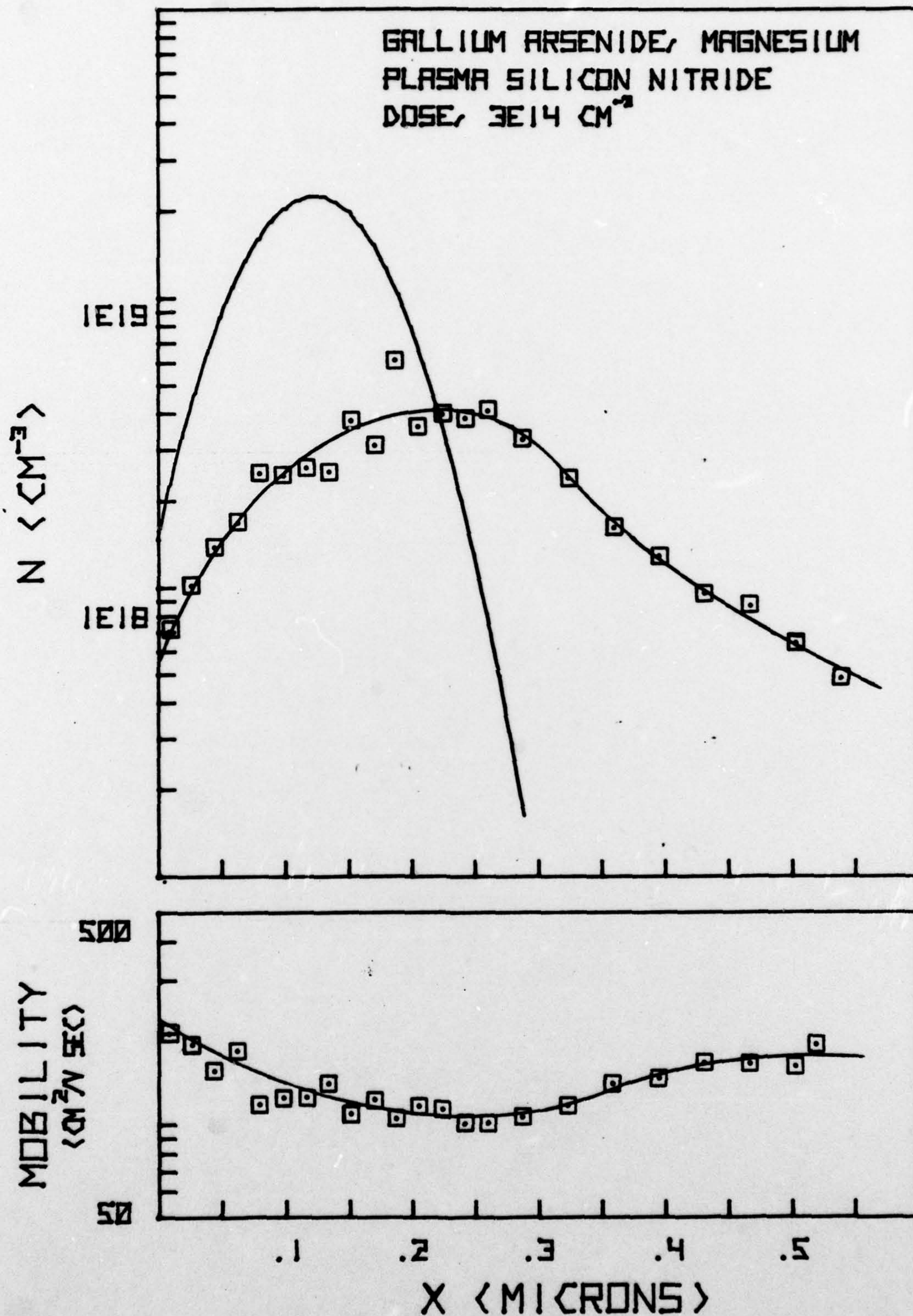

Figure 13. Carrier Concentration and Mobility Profile

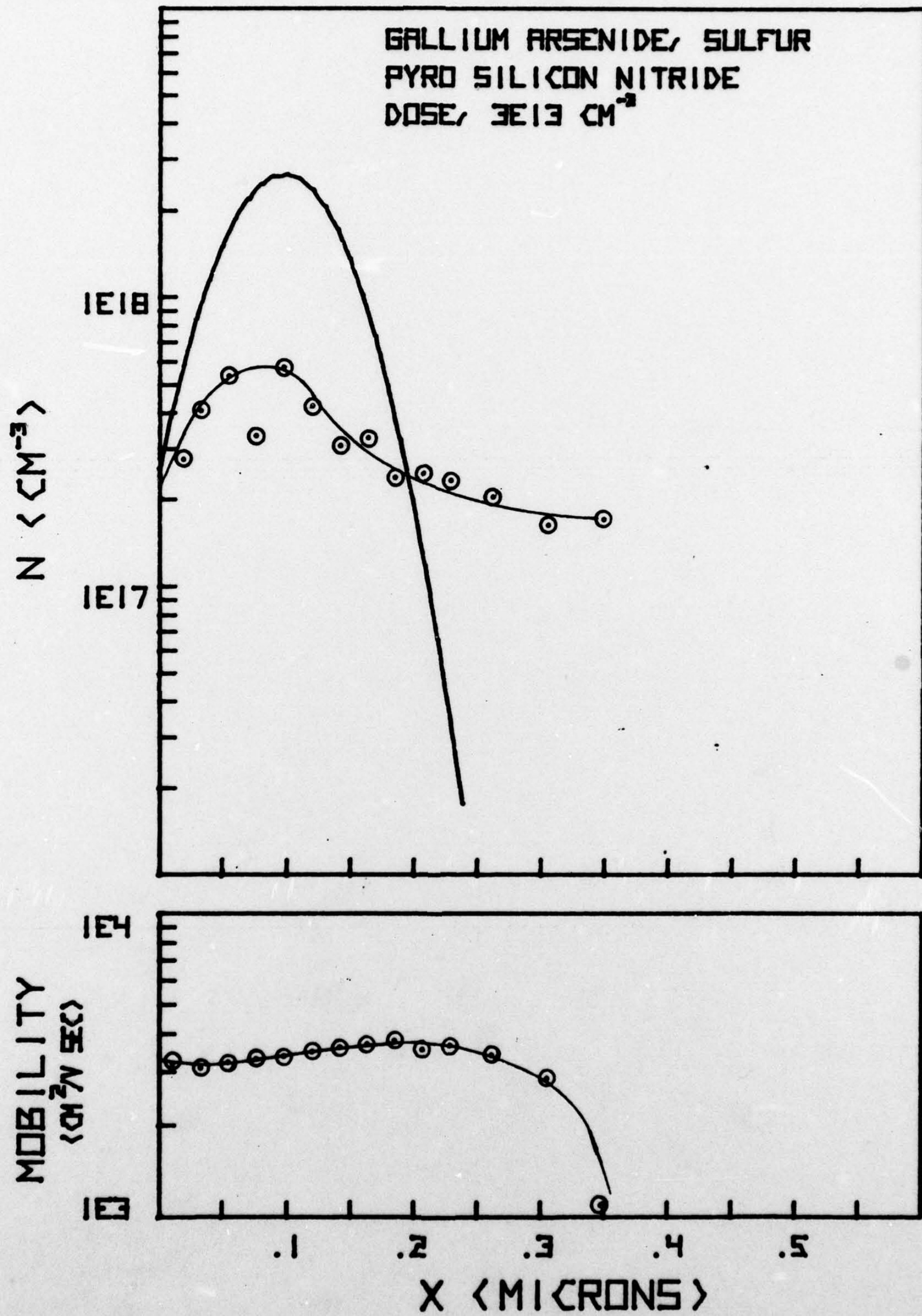

Figure 14. Carrier Concentration and Mobility Profile

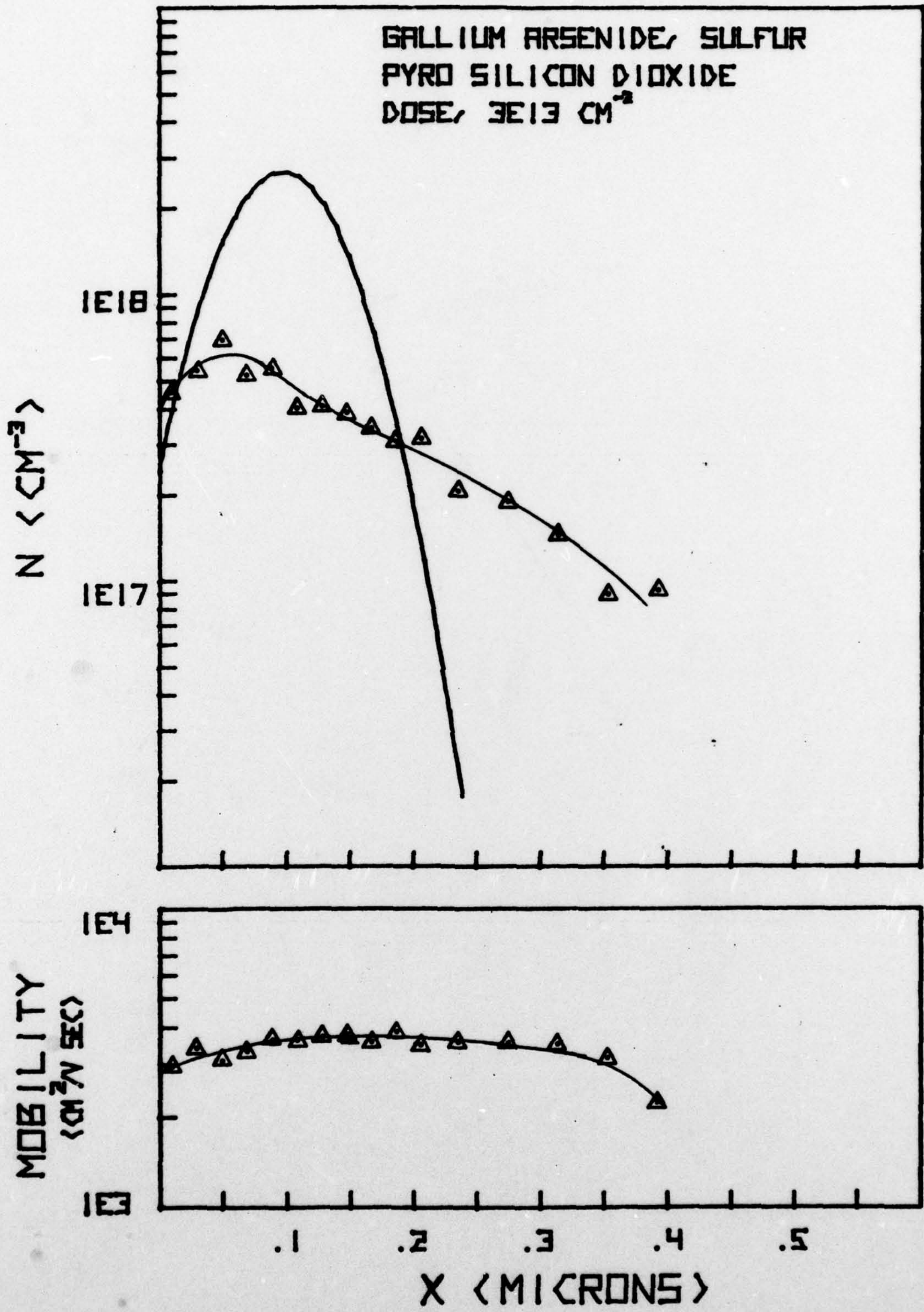

Figure 15. Carrier Concentration and Mobility Profile

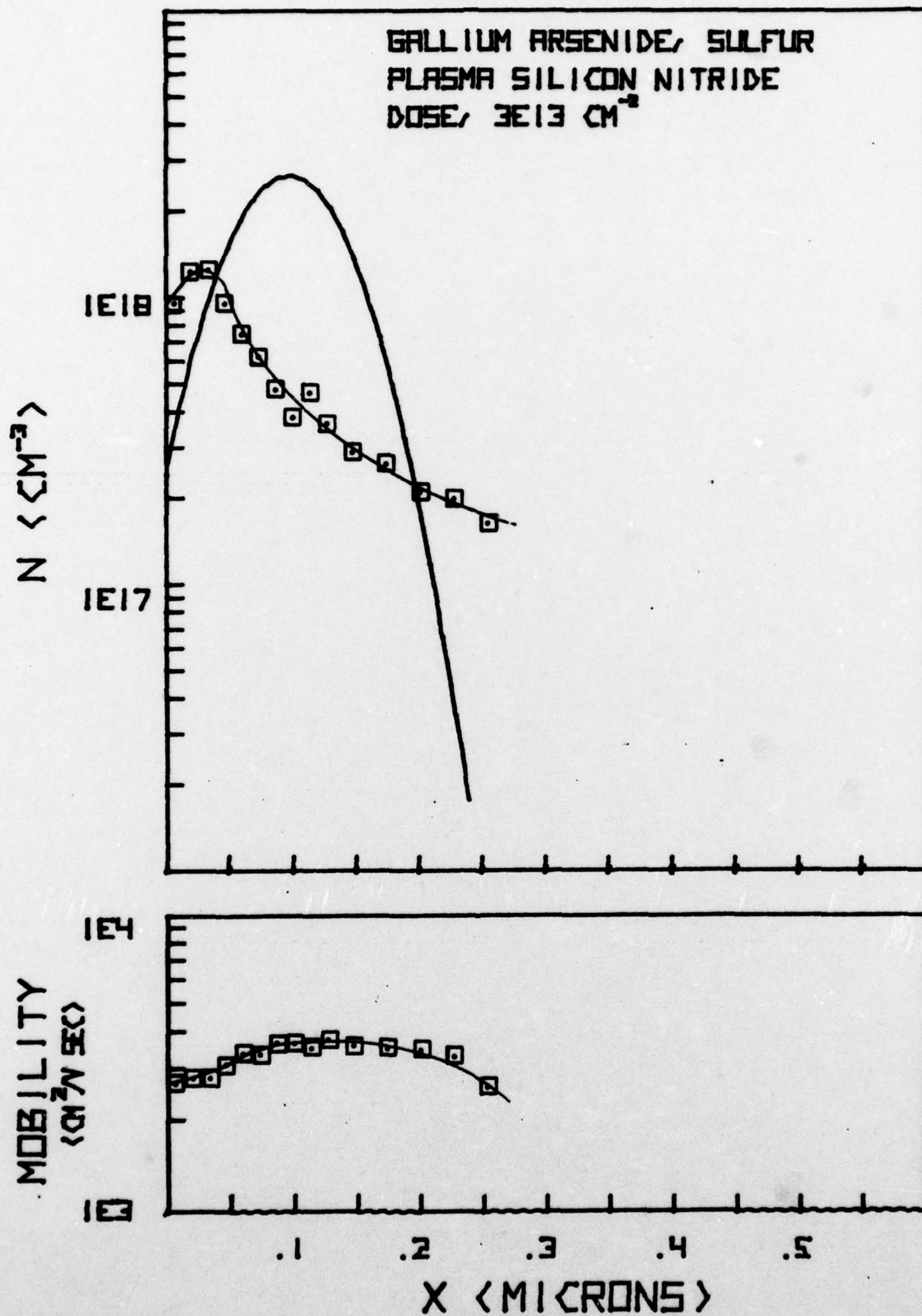

Figure 16. Carrier Concentration and Mobility Profile

VITA

Simeon Dewey Breault was born on 27 September 1952 in Lewiston, Maine. He graduated from high school in Lewiston in 1970 and entered Lowell University, in Lowell, Massachusetts, from which he received a Bachelor of Science degree with high honors in May 1974. Upon graduation, he was commissioned in the USAF through the ROTC program. After entering active duty in July 1974, he served as an Electronics Intelligence Analyst for the Foreign Technology Division of AF Systems Command at Wright-Patterson AFB, Ohio until entering the Air Force Institute of Technology, School of Engineering, in July 1977.

Permanent address:
209 Webster St.
Lewiston, Maine 04240

UNCLASSIFIED

SECURITY CLASSIFICATION OF THIS PAGE (When Data Entered)

REPORT DOCUMENTATION PAGE (14)		READ INSTRUCTIONS BEFORE COMPLETING FORM
1. REPORT NUMBER AFIT/GE/EE/78-19	2. GOVT ACCESSION NO. (9)	3. RECIPIENT'S CATALOG NUMBER Master's thesis
4. TITLE (and Subtitle) ELECTRICAL EFFECTS OF THREE DIFFERENT ENCAPSULANTS ON ION IMPLANTED GaAs.		5. TYPE OF REPORT & PERIOD COVERED MS Thesis
		6. PERFORMING ORG. REPORT NUMBER
7. AUTHOR(s) (10) Simeon Dewey Breault Captain USAF		8. CONTRACT OR GRANT NUMBER(s) (12) 63p.
9. PERFORMING ORGANIZATION NAME AND ADDRESS Air Force Institute of Technology(AFIT-EN) Wright-Patterson AFB, Ohio 45433		10. PROGRAM ELEMENT, PROJECT, TASK AREA & WORK UNIT NUMBERS
11. CONTROLLING OFFICE NAME AND ADDRESS Air Force Avionics Laboratory (DHR) Wright-Patterson AFB, Ohio 45433		12. REPORT DATE (11) December 1978
		13. NUMBER OF PAGES 62
14. MONITORING AGENCY NAME & ADDRESS(if different from Controlling Office)		15. SECURITY CLASS. (of this report) Unclassified
		15a. DECLASSIFICATION/DOWNGRADING SCHEDULE

16. DISTRIBUTION STATEMENT (of this Report)

Approved for public release; distribution unlimited.

17. DISTRIBUTION STATEMENT (of the abstract entered in Block 20, if different from Report)

18. SUPPLEMENTARY NOTES

Approved for public release; IAW AFR 190-17

Joseph P. Hipps, Major, USAF
Director of Information 1-23-79

19. KEY WORDS (Continue on reverse side if necessary and identify by block number)

Gallium Arsenide
Differential Hall Profiling
Electrical Activation
Van der Pauw Method
Mg-implanted GaAs
S-implanted GaAs
Ion Implantation
Encapsulation Effects

20. ABSTRACT (Continue on reverse side if necessary and identify by block number)

A compararive study was done of the effectiveness of three different encapsulants for annealing ion-implanted GaAs. The three encapsulants studied were pyrolitic Si_3N_4 and SiO_2, and plasma Si_3N_4. The study was limited to magnesium and sulfur implants done at room temperature with an implant energy of 120 keV. The implants were made into Cr-doped, semi-insulating substrates to doses ranging from $3x10^{12}$ to $1x10^{15}$ ions/cm^2. Annealing was done in a flowing H_2 atmosphere at 850°C for 15 minutes. Comparisons of

DD FORM 1 JAN 73 1473 EDITION OF 1 NOV 65 IS OBSOLETE

UNCLASSIFIED

SECURITY CLASSIFICATION OF THIS PAGE (When Data Entered)

next page

3 times 10 to the 12th power ← 10 to the 15th power

012 225

(Block 20, cont.) effectiveness were made on the basis of electrical activation efficiency and electrical profile measurements which were taken using a guarded Van der Pauw measurement system.

There was not a great deal of difference in the observed electrical activation efficiencies produced by the three different encapsulants. Plasma Si_3N_4 caps generally produced the highest activations, but were prone to pitting during annealing. The three encapsulants produced nearly identical electrical profiles, both for Mg and S implants. Contrary to previous studies, pyrolitic SiO_2 caps produced higher activations than pyrolitic Si_3N_4 caps for some doses of the S implants.